High Order Asymptotic Preserving DG-IMEX Schemes for Discrete-Velocity Kinetic Equations in a Diffusive Scaling

Juhi Jang [1] Fengyan Li [2] Jing-Mei Qiu [3] Tao Xiong [4]

Abstract

In this paper, we develop a family of high order asymptotic preserving schemes for some discrete-velocity kinetic equations under a diffusive scaling, that in the asymptotic limit lead to macroscopic models such as the heat equation, the porous media equation, the advection-diffusion equation, and the viscous Burgers' equation. Our approach is based on the micro-macro reformulation of the kinetic equation which involves a natural decomposition of the equation to the equilibrium and non-equilibrium parts. To achieve high order accuracy and uniform stability as well as to capture the correct asymptotic limit, two new ingredients are employed in the proposed methods: discontinuous Galerkin (DG) spatial discretization of arbitrary order of accuracy with suitable numerical fluxes; high order globally stiffly accurate implicit-explicit (IMEX) Runge-Kutta scheme in time equipped with a properly chosen implicit-explicit strategy. Formal asymptotic analysis shows that the proposed scheme in the limit of $\varepsilon \to 0$ is a consistent high order discretization for the limiting equation. Numerical results are presented to demonstrate the stability and high order accuracy of the proposed schemes together with their performance in the limit. Our methods are also tested for the continuous-velocity one-group transport equation in slab geometry and for several examples with spatially varying parameters.

Keywords: Kinetic equations; Asymptotic preserving; High order; DG-IMEX schemes

[1]Department of Mathematics, University of California Riverside, Riverside, CA 92521. E-mail: juhijang@math.ucr.edu. Supported in part by NSF grants DMS-0908007 and DMS-1212142.

[2]Department of Mathematical Sciences, Rensselaer Polytechnic Institute, Troy, NY 12180. E-mail: lif@rpi.edu. Supported in part by NSF grants DMS-0847241 and DMS-1318409.

[3]Department of Mathematics, University of Houston, Houston, 77204. E-mail: jingqiu@math.uh.edu. The third and fourth authors are supported in part by Air Force Office of Scientific Computing YIP grant FA9550-12-0318, NSF grant DMS-0914852 and DMS-1217008.

[4]Department of Mathematics, University of Houston, Houston, 77204. E-mail: txiong@math.uh.edu

1 Introduction

The evolution of particles in rarefied gas dynamics, neutron transport, radiative transfer or stellar dynamics can be modeled at different levels of scale. The microscopic particle dynamics is described by Newton's laws of motion, while the macroscopic hydrodynamics can model the observables such as density, velocity or temperature. Kinetic theory concerns the statistical description of particles via the particle density distribution rather than individual particles. The number of particles is typically more than 10^{20} and the computation, for instance in nanotechnology, is very expensive. In such situations, kinetic theory can be used to capture important properties of microscopic phenomena with reasonable computational cost. On the other hand, kinetic models often provide more detailed description than the macroscopic ones.

Kinetic theory is at the center of multi-scale modeling connecting the invisible microscopic models with the macroscopic models. In particular, when the mean free path of particles is sufficiently small, the system is close to the equilibrium state and it can be shown that a macroscopic model is a good approximation to the kinetic equation. Building a passage from kinetic to macroscopic models is a very interesting problem and there has been a lot of mathematical progress over the decades [2, 33].

Due to the relatively small yet multiple scales of particle interactions, developing efficient and effective kinetic simulation tools is mathematically and numerically challenging. For instance, non-thermal chemical equilibrium flow often displays multiple scales, requiring a hierarchy of physical models that range from kinetic theory to continuum fluid dynamics. To address multi-scale phenomena, there are hybrid domain decomposition method [7, 12], asymptotic preserving (AP) method [18, 30], moment method [25, 11, 8] etc. A goal shared by many of these multi-scale approaches is to resolve the physics of interest, e.g. macroscopic quantities, while avoiding the computational cost as much as possible to resolve small scale structures. In particular, for a kinetic equation with a broad range of Knudsen number ε that characterizes the kinetic scale, AP methods are designed to be uniformly stable with respect to ε, while mimicking the asymptotic limit from the kinetic to the hydrodynamic models on the PDE level as ε goes to 0. As a result, the scheme in the limit of $\varepsilon \to 0$ becomes a consistent discretization of the limiting macro-scale equations. The methods have been actively pursued by many researchers in recent years since they can effectively deal with multi-scales and capture hydrodynamic macro-scale limits in a uniform setting. We refer readers to [18, 30] for a review of the subject.

The focus of this paper is to design high order AP schemes for some discrete-velocity kinetic equations [20] under a diffusive scaling. It was shown in [19, 28] that improper treatment of spatial discretization even with a stable implicit time discretization may fail to capture the correct asymptotic limit, when the spatial and temporal mesh sizes do not resolve the ε-scale. In [19], by building in the correct asymptotic behavior, a scheme capturing the correct asymptotic limit with under-resolved mesh size was designed. In [28, 20], a proper splitting between the convection and stiff source terms was introduced to ensure the AP property; later the scheme was coupled with a second order Runge-Kutta splitting method and extended to continuous-velocity models based on the even and odd parities of the equation in [21]. In [22], an AP scheme was designed based on a standard perturbation procedure, followed by a fractional step scheme with a semi-implicit procedure. Based on the micro-macro decomposition, a first order finite difference AP method was formulated in [24] for staggered grids, and its stability and error estimates were established in [26]. Some new splitting strategies were proposed in [4, 6], with the focus on the design of various high order globally stiffly accurate implicit-explicit (IMEX) schemes.

In this paper, we propose a family of high order schemes for the discrete-velocity kinetic equations as an initial effort in designing high order simulation tools for more general kinetic equations under different scalings. What we proposed in this paper, for the first time, combines several state-of-art ingredients: (1) PDE decomposition of micro-macro components, (2) discontinuous Galerkin (DG) methods that can be designed to be arbitrarily high order accurate, and are compact and very flexible for h-p adaptivity, (3) globally stiffly accurate IMEX Runge-Kutta (RK) time discretization to preserve AP properties of the system. These key ingredients, together with suitable design for numerical fluxes and implicit-explicit strategies, offer a unified framework for high order schemes. Formal asymptotic analysis shows that the proposed methods, as Knudsen number ε goes to 0, become consistent high order discretizations for the limiting macro-scale equations. These limiting schemes specifically involve (local) DG spatial discretizations and RK methods in time, if the initial condition is well-prepared. Numerical results further demonstrate the stability and high order accuracy of the proposed schemes when ε is of order 1 and in the limit of ε goes to 0. Both linear and nonlinear problems are considered with some smooth and non-smooth solutions. We also test our schemes for the continuous-velocity one-group transport equation in slab geometry, and for several examples in mixed regimes with spatially varying parameters. In a companion paper [16], some theoretical results are established in terms of uniform stability of the schemes, the error estimate for smooth solutions, as well as rigorous asymptotic analysis.

Micro-macro decomposition is originated by the theoretical PDE community (for instance, see [27]) in trying to solve the collisional kinetic equations such as Boltzmann equation, and it has been successfully used to extract the structure of dissipation and the interaction between the equilibrium and the non-equilibrium parts. We advocate the micro-macro decomposition framework as it provides a general guidance on how to perform spatial discretization with proper inter-element treatments, and on how to discretize in time with a suitable implicit-explicit strategy for different terms to achieve desired uniform stability. It is based on projection, and therefore provides a natural framework for projection-based discretizations such as DG methods. DG methods are a class of finite element methods which use discontinuous approximating functions, they have been designed for a wide range of equations and gain popularity in many areas of science and engineering [9, 15, 31]. DG methods provide a framework to systematically design schemes with arbitrary order of accuracy. Some other attractive properties include their flexibility with general meshes and local approximations hence suitability for h-p adaptivity, compactness, being highly parallelable, ease of handling various boundary conditions, and provable stability and error estimates for many linear and nonlinear problems [17, 10]. For high-order differential equations such as the diffusion equation, local DG methods were developed based on rewriting the system into its first order form [9, 34]. For the stationary radiative transfer equations, an AP scheme based on an upwind DG discretization was analyzed in [14]. To discretize in time, we apply globally stiffly accurate IMEX RK methods [4] which rely on an implicit-explicit strategy different from that in [24]. IMEX schemes were developed, analyzed, and applied to hyperbolic system with relaxation and in the diffusive limit in [29, 3, 5, 4]. It was shown that high order temporal accuracy can be achieved for both $\varepsilon = O(1)$ and $\varepsilon \ll 1$. Our IMEX strategy and the globally stiffly accurate property of IMEX schemes ensure the correct asymptotic limit of numerical solutions from internal stages of RK methods and at each discrete time.

The paper is organized as follows. In Section 2, we introduce the discrete-velocity kinetic equation, and provide examples we will consider as well as their micro-macro decomposition and diffusive limits. In Section 3, a family of (formally) high order schemes are proposed, they

employ DG spatial discretization with suitable numerical fluxes and globally stiffly accurate IMEX RK temporal discretization. Formal asymptotic analysis is then performed when $\varepsilon \to 0$ for the proposed methods. In Section 4, numerical results are presented. High order accuracy is observed as designed with ε's ranging from 10^{-6} to $O(1)$, together with the correct asymptotic behavior for $\varepsilon \to 0$. In Section 5, the proposed schemes are applied to the one-group transport equation in slab geometry. High order accuracy, as well as the robustness in resolving multi-scale features in transport and diffusive regimes, are demonstrated through several numerical examples. Finally, conclusions are made in Section 6.

2 Formulation

We consider the following discrete-velocity kinetic model in a diffusive scaling

$$\varepsilon \partial_t f + v \cdot \nabla_x f = \frac{1}{\varepsilon} \mathcal{C}(f) \tag{2.1}$$

with the initial data f_0 and suitable boundary conditions, where $f = f(x, v, t)$ is the distribution function of particles that depends on time $t > 0$, position $x \in \Omega_x \subset \mathbb{R}$, and velocity $v \in \{-1, 1\}$. The parameter $\varepsilon > 0$ measures the distance of the system to the equilibrium state and it can be regarded as the mean free path of the particles; when ε is small, the system is close to equilibrium; when ε is large, the system is far from equilibrium. $\mathcal{C}(f)$ is a collision operator that describes the interactions of particles among themselves and with the medium.

The following are interesting examples of $\mathcal{C}(f)$ that we will focus on in this paper:

$$\mathcal{C}(f) = \langle f \rangle - f, \tag{2.2a}$$
$$\mathcal{C}(f) = K \langle f \rangle^m \left(\langle f \rangle - f \right), \quad K > 0 \text{ and } m \leq 0, \tag{2.2b}$$
$$\mathcal{C}(f) = \langle f \rangle - f + A\varepsilon v \langle f \rangle, \quad |A\varepsilon| < 1, \tag{2.2c}$$
$$\mathcal{C}(f) = \langle f \rangle - f + C\varepsilon \left[\langle f \rangle^2 - (\langle f \rangle - f)^2 \right] v, \quad C > 0. \tag{2.2d}$$

Here $\langle f \rangle := \int f d\mu$ where $d\mu$ is the discrete Lebesgue measure on $\{-1, 1\}$:

$$\langle f \rangle = \frac{f(x, v = 1, t) + f(x, v = -1, t)}{2}.$$

We remark that the equation (2.1) with (2.2a)-(2.2d) was extensively studied in [20]. It was rewritten as the system of two equations for $u_1(x, t) = f(x, v = 1, t)$ and $u_2(x, t) = f(x, v = -1, t)$. In particular, this new system with the collision operator (2.2a) is known as the one-dimensional Goldstein-Taylor model or the telegraph equation. In this paper, we will design high order numerical schemes for (2.1) with (2.2a)-(2.2d) based on its micro-macro decomposition.

2.1 Micro-macro formulation

Note that $\langle 1 \rangle = 1$ and $\langle v \rangle = 0$ and we view 1 as the equilibrium state. We consider the Hilbert space $L^2(d\mu)$ in v variable with the following inner product: $\langle f, g \rangle := \int f g d\mu = \langle fg \rangle$ and introduce the orthogonal projection operator Π onto Span(1). The micro-macro decomposition is performed in two steps: first to write f by using the orthogonal projections Π and $\mathbf{I} - \Pi$: $f = \Pi f + (\mathbf{I} - \Pi) f$ where Πf is the macroscopic part (equilibrium part of f) and $(\mathbf{I} - \Pi) f$ is the microscopic part (the non-equilibrium part of f) so that $\Pi f = \langle f \rangle \cdot 1$ and $\langle (\mathbf{I} - \Pi) f, 1 \rangle = 0$,

and then to decompose the kinetic equation via the projections in terms of Πf and $(\mathbf{I}-\Pi)f$. Here $\mathbf{I}$ is the identity operator.

In order to describe the micro-macro formulation for (2.1), we introduce $\rho := \langle f\rangle = \Pi f$ to denote the macroscopic density for f and consider the following orthogonal decomposition,

$$f = \langle f\rangle + \varepsilon g = \rho + \varepsilon g \tag{2.3}$$

where $\langle g\rangle = 0$. Note that $\langle \mathcal{C}(f)\rangle = 0$ for (2.2a)–(2.2d). Then the projection Π of (2.1) gives rise to $\varepsilon\partial_t\langle f\rangle + \partial_x\langle vf\rangle = 0$. On the other hand, $\langle g\rangle = 0$ and $\langle v\rho\rangle = \rho\langle v\rangle = 0$, hence we obtain

$$\partial_t\rho + \partial_x\langle vg\rangle = 0.$$

Next, we apply $(\mathbf{I}-\Pi)$ to (2.1) and get

$$\varepsilon^2\partial_t g + v\partial_x\rho + \varepsilon(\mathbf{I}-\Pi)(v\partial_x g) = \frac{1}{\varepsilon}(\mathbf{I}-\Pi)\mathcal{C}(f) = \frac{1}{\varepsilon}\mathcal{C}(\rho+\varepsilon g).$$

Here $\langle \mathcal{C}(f)\rangle = 0$ is used. The micro-macro decomposition now yields the set of two equations

$$\begin{aligned} &\partial_t\rho + \partial_x\langle vg\rangle = 0,\\ &\partial_t g + \frac{1}{\varepsilon}(\mathbf{I}-\Pi)(v\partial_x g) + \frac{1}{\varepsilon^2}v\partial_x\rho = \frac{1}{\varepsilon^3}\mathcal{C}(\rho+\varepsilon g). \end{aligned} \tag{2.4}$$

The solvability for f of (2.1) and the solvability for ρ and g of (2.4) are equivalent.

For our two-velocity model, by writing $j(x,t) := \frac{1}{2\varepsilon}(f(x,v=1,t) - f(x,v=-1,t))$, the micro-macro decomposition (2.4) can be put into the following form:

$$\partial_t\rho + \partial_x j = 0\,,\ \ \varepsilon^2\partial_t j + \partial_x\rho = \mathcal{S}(\rho, j) \tag{2.5}$$

where $\mathcal{S}(\rho, j)$ depends on $\mathcal{C}(f)$.

Remark 2.1. In a more general setting where the parameter ε depends on the position x: $\varepsilon = \varepsilon(x)$, the micro-macro formulation (2.4) could be written as follows:

$$\begin{aligned} &\varepsilon(x)\partial_t\rho + \partial_x\left(\varepsilon(x)\langle vg\rangle\right) = 0,\\ &\varepsilon(x)^2\partial_t g + (\mathbf{I}-\Pi)\big(v\partial_x(\varepsilon(x)g)\big) + v\partial_x\rho = \frac{1}{\varepsilon(x)}\mathcal{C}(\rho+\varepsilon(x)g). \end{aligned} \tag{2.6}$$

2.2 Diffusive limit and some energy identities

In this subsection, we will derive the equations that ρ would satisfy in the limit of $\varepsilon\to 0$. Energy identities will also be given for some cases.

• Heat and porous media equations. We will treat (2.2a) and (2.2b) together by regarding (2.2a) as a special case of (2.2b) with $m=0$ and $K=1$. It is clear that

$$\mathcal{C}(f) = \mathcal{C}(\rho+\varepsilon g) = -K\varepsilon\rho^m g. \tag{2.7}$$

To see the limiting equation for ρ, we take the second equation in (2.4), write it as $g = -\frac{1}{K(1-m)}v\partial_x(\rho^{1-m}) + O(\varepsilon)$ and plug it into the first equation in (2.4) to obtain

$$\partial_t\rho = \frac{1}{K(1-m)}\partial_{xx}\left(\rho^{1-m}\right) + O(\varepsilon).$$

This will lead to a family of diffusion equations for ρ as $\varepsilon \to 0$. If $m = 0$, the limiting equation is the linear heat equation; if $m < 0$, it is the slow (nonlinear) diffusion equation, known as the porous media equation.

With j notation, we see that $\mathcal{S}(\rho, j) = -K\rho^m j$ and it is straightforward to check that the solutions to (2.5) in a periodic domain satisfy the following energy identity:

$$\frac{1}{2}\frac{d}{dt}\int(\rho^2 + \varepsilon^2 j^2)dx + \int K\rho^m j^2 dx = 0$$

which indicates the dissipation mechanism of the system.

• Advection-diffusion equation. From (2.2c), we see that

$$\mathcal{C}(f) = \mathcal{C}(\rho + \varepsilon g) = -\varepsilon(g - Av\rho). \tag{2.8}$$

By writing $g = Av\rho - v\partial_x\rho + O(\varepsilon)$ and plugging it into the first equation in (2.4), we recover an advection-diffusion equation for ρ as $\varepsilon \to 0$:

$$\partial_t\rho + A\partial_x\rho = \partial_{xx}\rho. \tag{2.9}$$

As in the previous case, some dissipation mechanism is expected, but we haven't found any specific results written in the literature. In the following, we present the L^2 stability result.

Proposition 2.2. Suppose ρ and j satisfy (2.5) with $\mathcal{S}(\rho, j) = -j + A\rho$ in a periodic domain. Then ρ and j obey the following energy identity:

$$\frac{1}{2}\frac{d}{dt}\int\left[(1 - \varepsilon^2 A^2)\rho^2 + \varepsilon^2(j - A\rho)^2\right]dx + \int(j - A\rho)^2 dx = 0. \tag{2.10}$$

Proof. Since $j - A\rho$ rather than j drives the system dissipate, we will try to derive the energy identity for ρ and $j - A\rho$. Multiply the first equation in (2.5) by ρ and the second equation by $j - A\rho$, and integrate over x to get

$$\underbrace{\int \partial_t\rho\rho dx}_{=\frac{1}{2}\frac{d}{dt}\int\rho^2 dx} + \underbrace{\int \varepsilon^2\partial_t j(j - A\rho)dx}_{(a)} + \underbrace{\int \partial_x j\rho dx + \int \partial_x\rho(j - A\rho)dx}_{(b)} = -\int(j - A\rho)^2 dx.$$

Notice that

$$\begin{aligned}(a) &= \int \varepsilon^2\partial_t(j - A\rho)(j - A\rho)dx + \int \varepsilon^2 A\partial_t\rho j dx - \int \varepsilon^2 A\partial_t\rho A\rho dx \\ &= \frac{1}{2}\frac{d}{dt}\int \varepsilon^2\left[(j - A\rho)^2 - (A\rho)^2\right]dx - \underbrace{\int \varepsilon^2 A\partial_x jj dx}_{=0}, \\ (b) &= \int \partial_x(j\rho - \frac{A\rho^2}{2})dx = 0 \ \text{ (integration by parts).}\end{aligned}$$

Hence, we obtain (2.10). □

We observe that as long as $|\varepsilon A| < 1$, the positivity of the energy in (2.10) is guaranteed. The energy identity (2.10) gives rise to the L^2 energy law for the advection-diffusion equation $\partial_t \rho + A\partial_x \rho = \partial_{xx}\rho$ in the limit of $\varepsilon \to 0$.

• Viscous Burgers' equation. For (2.2d), we notice that

$$\mathcal{C}(f) = \mathcal{C}(\rho + \varepsilon g) = -\varepsilon g + C\varepsilon \left[\rho^2 - \varepsilon^2 g^2\right] v. \tag{2.11}$$

We write $g = Cv\rho^2 - v\partial_x \rho + O(\varepsilon)$ and plug it into the first equation in (2.4) to get

$$\partial_t \rho + C\partial_x(\rho^2) = \partial_{xx}\rho + O(\varepsilon),$$

which yields a viscous Burgers' equation for ρ as $\varepsilon \to 0$.

The corresponding equations (2.5) can be obtained with $\mathcal{S}(\rho, j) = -j + C[\rho^2 - \varepsilon^2 j^2]$. This model is known as the nonlinear Ruijgrok-Wu model [32].

3 DG-IMEX Methods

In this section, we will propose a family of high order methods for the discrete-velocity kinetic equation (2.1) based on its micro-macro reformulation (2.4). The methods involve discontinuous Galerkin (DG) discretization of arbitrary order of accuracy in space and globally stiffly accurate implicit-explicit (IMEX) Runge-Kutta (RK) methods in time. Formal asymptotic analysis is performed to show that the proposed schemes in the limit of $\varepsilon \to 0$ become consistent high order schemes for the limiting equations.

3.1 DG spatial discretizations

We first discretize the micro-macro system (2.4) in space by DG methods. Since the discrete-velocity models considered here do not admit boundary layers, for brevity of presentation, we assume the boundary condition in x is periodic and $\Omega_x = [x_{\min}, x_{\max}]$. Other types of boundary conditions can be easily treated. Our spatial discretization is formulated on one mesh. Let's first introduce some notation. Start with $\{x_{i+\frac{1}{2}}\}_{i=0}^{i=N}$, a partition of Ω_x. Here $x_{\frac{1}{2}} = x_{\min}$, $x_{N+\frac{1}{2}} = x_{\max}$, each element is denoted as $I_i = [x_{i-\frac{1}{2}}, x_{i+\frac{1}{2}}]$ with its length Δx_i, and $\Delta x = \max_i \Delta x_i$. Given any non-negative integer k, we define a finite dimensional discrete space

$$U_h^k = \left\{u \in L^2(\Omega_x) : u|_{I_i} \in P^k(I_i), \forall i\right\}. \tag{3.1}$$

The local space $P^k(I)$ consists of polynomials of degree at most k on I. Note functions in U_h^k are piecewise-defined, and they are double-valued at grid points. For such functions, notation is introduced for jump and average: with $u(x^{\pm}) = \lim_{\Delta x \to 0^{\pm}} u(x + \Delta x)$, the jump and the average of u at $x_{i+\frac{1}{2}}$ are defined as $[u]_{i+\frac{1}{2}} = u(x^+_{i+\frac{1}{2}}) - u(x^-_{i+\frac{1}{2}})$ and $\{u\}_{i+\frac{1}{2}} = \frac{1}{2}(u(x^+_{i+\frac{1}{2}}) + u(x^-_{i+\frac{1}{2}}))$, respectively. We also use $u_{i+\frac{1}{2}} = u(x_{i+\frac{1}{2}})$, $u^{\pm}_{i+\frac{1}{2}} = u(x^{\pm}_{i+\frac{1}{2}}), \forall i$.

We are now ready to define the semi-discrete DG method for the micro-macro system (2.4).

Look for $\rho_h(\cdot,t), g_h(\cdot,v,t) \in U_h^k$, such that $\forall \phi, \psi \in U_h^k$, and $\forall i$,

$$\int_{I_i} \partial_t \rho_h \phi dx - \int_{I_i} \langle v g_h \rangle \partial_x \phi dx + \widehat{\langle v g_h \rangle}_{i+\frac{1}{2}} \phi^-_{i+\frac{1}{2}} - \widehat{\langle v g_h \rangle}_{i-\frac{1}{2}} \phi^+_{i-\frac{1}{2}} = 0, \tag{3.2a}$$

$$\begin{aligned}\int_{I_i} \partial_t g_h \psi dx + \frac{1}{\varepsilon} \int_{I_i} (\mathbf{I} - \Pi) \mathcal{D}_h(g_h; v)\, \psi dx - \frac{1}{\varepsilon^2} \left(\int_{I_i} v \rho_h \partial_x \psi dx - v \widehat{\rho}_{h,i+\frac{1}{2}} \psi^-_{i+\frac{1}{2}} + v \widehat{\rho}_{h,i-\frac{1}{2}} \psi^+_{i-\frac{1}{2}} \right) \\ = \frac{1}{\varepsilon^3} \int_{I_i} \mathcal{C}(\rho_h + \varepsilon g_h) \psi dx.\end{aligned} \tag{3.2b}$$

In (3.2b), $\mathcal{D}_h(g_h; v) \in U_h^k$, and it is determined by an upwind discretization of $v\partial_x g$ within the DG framework,

$$\begin{aligned}(\mathcal{D}_h(g_h; v), \psi) &= \sum_i \left(- \int_{I_i} v g_h \partial_x \psi dx + \widetilde{(v g_h)}_{i+\frac{1}{2}} \psi^-_{i+\frac{1}{2}} - \widetilde{(v g_h)}_{i-\frac{1}{2}} \psi^+_{i-\frac{1}{2}} \right) \\ &= -\sum_i \left(\int_{I_i} v g_h \partial_x \psi dx \right) - \sum_i \widetilde{(v g_h)}_{i-\frac{1}{2}} [\psi]_{i-\frac{1}{2}}, \quad \psi \in U_h^k,\end{aligned} \tag{3.3}$$

where $\widetilde{vg}$ is an upwind numerical flux consistent to vg,

$$\widetilde{vg} := \begin{cases} vg^-, & \text{if } v > 0 \\ vg^+, & \text{if } v < 0 \end{cases} = v\{g\} - \frac{|v|}{2}[g]. \tag{3.4}$$

Here and below, the standard inner product $(\cdot,\cdot)$ for the $L^2(\Omega_x)$ space is used, see the first term in (3.3).

Both $\widehat{\langle vg \rangle}$ and $\hat{\rho}$ in (3.2) are also numerical fluxes, and they are consistent to the physical ones $\langle vg \rangle$ and ρ. In this paper, we consider the following three choices:

$$\text{alternating left-right:} \quad \widehat{\langle vg \rangle} = \langle vg \rangle^-, \hat{\rho} = \rho^+ , \tag{3.5a}$$

$$\text{alternating right-left:} \quad \widehat{\langle vg \rangle} = \langle vg \rangle^+, \hat{\rho} = \rho^- , \tag{3.5b}$$

$$\text{central:} \quad \widehat{\langle vg \rangle} = \{\langle vg \rangle\}, \hat{\rho} = \{\rho\} . \tag{3.5c}$$

Compared with central flux, alternating flux will result in a scheme with smaller dependant stencil. For different collision kernels $\mathcal{C}(f)$ in (2.2), choices of fluxes may vary with the consideration of the stability and accuracy of the algorithm. More specifically,

(1) For the linear equation (2.4) with (2.7) and $m = 0$, one can use any numerical flux given in (3.5).

(2) For the nonlinear equation (2.4) with (2.7) and $m \neq 0$, as $\varepsilon \to 0$, the limiting equation is the porous media equation for ρ. When $\rho > 0$, the equation is diffusive. Similar to the linear case, we can choose any numerical flux given in (3.5). However, the equation becomes degenerate when $\rho = 0$, resulting in the phenomenon of finite speed propagation. Hence special attention has to be paid around the interface of $\rho = 0$ when the alternating flux is used. In particular, when the interface is moving towards right, alternating left-right flux is used; when the interface is moving towards left, alternating right-left flux is used. More details are given in Section 4.

(3) For the convection-diffusion equations (2.4) with (2.8) or (2.11), we choose the flux (3.5a) for $A > 0$ and for $C > 0$ (resp. the flux (3.5b) for $A < 0$ and for $C < 0$). Such choice ensures an upwind flux for the advective term in the limiting equation. When the convection is not dominating, central flux can also be used.

To get a more compact form of the scheme, one further sums up (3.2) with respect to i,

$$(\partial_t \rho_h, \phi) + a_h(g_h, \phi) = 0, \tag{3.6a}$$

$$(\partial_t g_h, \psi) + \frac{1}{\varepsilon} b_{h,v}(g_h, \psi) - \frac{v}{\varepsilon^2} d_h(\rho_h, \psi) = -\frac{1}{\varepsilon^2} s^{(1)}_{h,v}(\rho_h, g_h, \psi) - s^{(2)}_{h,v}(g_h, \psi), \tag{3.6b}$$

where

$$a_h(g_h, \phi) = -\sum_i \int_{I_i} \langle v g_h \rangle \partial_x \phi dx - \sum_i \widehat{\langle v g_h \rangle}_{i-\frac{1}{2}} [\phi]_{i-\frac{1}{2}}, \tag{3.7a}$$

$$b_{h,v}(g_h, \psi) = ((\mathbf{I} - \Pi)\mathcal{D}_h(g_h; v), \psi) = (\mathcal{D}_h(g_h; v) - \langle \mathcal{D}_h(g_h; v) \rangle, \psi), \tag{3.7b}$$

$$d_h(\rho_h, \psi) = \sum_i \int_{I_i} \rho_h \partial_x \psi dx + \sum_i \widehat{\rho}_{h,i-\frac{1}{2}} [\psi]_{i-\frac{1}{2}}, \tag{3.7c}$$

and

$$s^{(1)}_{h,v}(\rho_h, g_h, \psi) = \begin{cases} (K \rho_h^m g_h, \psi) & \text{for (2.7)} \\ (g_h - A v \rho_h, \psi) & \text{for (2.8)} \\ (g_h - C v \rho_h^2, \psi) & \text{for (2.11)} \end{cases}, s^{(2)}_{h,v}(g_h, \psi) = \begin{cases} 0 & \text{for (2.7)(2.8)} \\ (C v g_h^2, \psi) & \text{for (2.11).} \end{cases}$$

Note that the source term is written into a sum of two terms which are of different scales in ε. These two terms will be treated differently in time discretization, see Section 3.2.

Remark 3.1. For the two-velocity models considered here, one can easily verify that $(\mathbf{I} - \Pi)(v\partial_x g) = v\langle \partial_x g \rangle$ holds. Recall the exact solution satisfies $\langle \partial_x g \rangle = \partial_x \langle g \rangle = 0$, hence $(\mathbf{I} - \Pi)(v\partial_x g)$ should vanish and it does not seem one needs to discretize $(\mathbf{I} - \Pi)(v\partial_x g)$ numerically. The analysis in the companion paper [16], however, implies that it is important to keep this term in order to obtain a more desirable stability condition on the time step, $\Delta t = O(\varepsilon h)$, in the convective regime with $\varepsilon = O(1)$ instead of $\Delta t = O(h^2)$ otherwise.

3.2 Fully discrete DG-IMEX methods

In this subsection, the semi-discrete DG method is further discretized in time with globally stiffly accurate IMEX RK schemes. We start with first order accuracy in time. Given $\rho_h^n(\cdot),\ g_h^n(\cdot, v) \in U_h^k$ that approximate the solution ρ and g at $t = t^n$, we look for $\rho_h^{n+1}(\cdot),\ g_h^{n+1}(\cdot, v) \in U_h^k$, such that $\forall \phi, \psi \in U_h^k$,

$$\left(\frac{\rho_h^{n+1} - \rho_h^n}{\Delta t}, \phi\right) + a_h(g_h^n, \phi) = 0, \tag{3.8a}$$

$$\left(\frac{g_h^{n+1} - g_h^n}{\Delta t}, \psi\right) + \frac{1}{\varepsilon} b_{h,v}(g_h^n, \psi) - \frac{v}{\varepsilon^2} d_h(\rho_h^{n+1}, \psi) = -\frac{1}{\varepsilon^2} s^{(1)}_{h,v}(\rho_h^{n+1}, g_h^{n+1}, \psi) - s^{(2)}_{h,v}(g_h^n, \psi). \tag{3.8b}$$

We choose to use an implicit-explicit strategy different from that in [24], as it is natural to treat both the collisional and convective stiff terms in the scale of $\frac{1}{\varepsilon^2}$ implicitly. More importantly,

this strategy can be directly used for the higher order temporal discretizations as discussed next.

To achieve higher order accuracy in time, we adopt the globally stiffly accurate IMEX RK schemes [4]. Recall an IMEX RK scheme can be represented with a double Butcher tableau

$$\begin{array}{c|c} \tilde{c} & \tilde{\mathcal{A}} \\ \hline & \tilde{b}^T \end{array} \qquad \begin{array}{c|c} c & \mathcal{A} \\ \hline & b^T \end{array} \ , \tag{3.9}$$

where both $\tilde{\mathcal{A}} = (\tilde{a}_{ij})$ and $\mathcal{A} = (a_{ij})$ are $s \times s$ matrices, with $\tilde{\mathcal{A}}$ being lower triangular with zero diagonal entries. The coefficients $\tilde{c}$ and c are given by the usual relation $\tilde{c}_i = \sum_{j=1}^{i-1} \tilde{a}_{ij}$, $c_i = \sum_{j=1}^{i} a_{ij}$, and vectors $\tilde{b} = (\tilde{b}_j)$ and $b = (b_j)$ provide the quadrature weights to combine internal stages of the RK method. The IMEX RK scheme is said to be *globally stiffly accurate* [4] if

$$c_s = \tilde{c}_s = 1, \text{ and } \ a_{sj} = b_j, \tilde{a}_{sj} = \tilde{b}_j, \forall j = 1, \cdots, s. \tag{3.10}$$

The first order IMEX scheme employed in (3.8), represented by

$$\begin{array}{c|cc} 0 & 0 & 0 \\ 1 & 1 & 0 \\ \hline & 1 & 0 \end{array} \qquad \begin{array}{c|cc} 0 & 0 & 0 \\ 1 & 0 & 1 \\ \hline & 0 & 1 \end{array} \ ,$$

is globally stiffly accurate. In this work, we assume $\mathcal{A}$ in (3.9) is lower triangular to ensure efficient implementation. In addition, it is assumed that $\mathcal{A}$ either has nonzero diagonal entries, or has the following structure,

$$\begin{bmatrix} 0 & 0 \\ 0 & \hat{\mathcal{A}} \end{bmatrix}$$

where the diagonal entries of $\hat{\mathcal{A}}$ are nonzero. For the latter case, the corresponding IMEX RK method is called of type ARS [4].

Now we will apply a general globally stiffly accurate IMEX RK scheme, represented by (3.9) with the property (3.10), to the semi-discrete DG scheme (3.6). This is combined with the same implicit-explicit strategy as in the first order case, namely, the terms a_h, $b_{h,v}$ and $s^{(2)}_{h,v}$ in (3.6) are treated explicitly and the terms d_h, $s^{(1)}_{h,v}$ implicitly. Given $\rho^n_h(\cdot),\ g^n_h(\cdot, v) \in U^k_h$, we look for $\rho^{n+1}_h(\cdot),\ g^{n+1}_h(\cdot, v) \in U^k_h$, such that $\forall \phi, \psi \in U^k_h$,

$$\left(\rho^{n+1}_h, \phi\right) = (\rho^n_h, \phi) - \Delta t \sum_{l=1}^{s} \tilde{b}_l a_h(g^{(l)}_h, \phi), \tag{3.11a}$$

$$\begin{aligned} \left(g^{n+1}_h, \psi\right) = (g^n_h, \psi) &- \Delta t \sum_{l=1}^{s} \tilde{b}_l \left(\frac{1}{\varepsilon} b_{h,v}(g^{(l)}_h, \psi) + s^{(2)}_{h,v}(g^{(l)}_h, \psi) \right) \\ &+ \Delta t \sum_{l=1}^{s} \frac{b_l}{\varepsilon^2} \left(v d_h(\rho^{(l)}_h, \psi) - s^{(1)}_{h,v}(\rho^{(l)}_h, g^{(l)}_h, \psi) \right). \end{aligned} \tag{3.11b}$$

Here the approximations at the internal stages of an RK step, $\rho^{(l)}_h(\cdot),\ g^{(l)}_h(\cdot, v) \in U^k_h$ with

$l = 1, \cdots, s$, satisfy

$$\left(\rho_h^{(l)}, \phi\right) = (\rho_h^n, \phi) - \Delta t \sum_{j=1}^{l-1} \tilde{a}_{lj} a_h(g_h^{(j)}, \phi), \tag{3.12a}$$

$$\begin{aligned}\left(g_h^{(l)}, \psi\right) = (g_h^n, \psi) &- \Delta t \sum_{j=1}^{l-1} \tilde{a}_{lj} \left(\frac{1}{\varepsilon} b_{h,v}(g_h^{(j)}, \psi) + s_{h,v}^{(2)}(g_h^{(j)}, \psi)\right) \\ &+ \Delta t \sum_{j=1}^{l} \frac{a_{lj}}{\varepsilon^2} \left(v d_h(\rho_h^{(j)}, \psi) - s_{h,v}^{(1)}(\rho_h^{(j)}, g_h^{(j)}, \psi)\right)\end{aligned} \tag{3.12b}$$

for any $\phi, \psi \in U_h^k$.

The property of being globally stiffly accurate guarantees that the updated numerical solution at t^{n+1} is the same as the one from the last internal stage of one RK step. That is, one can equivalently replace equations in (3.11) by

$$\rho_h^{n+1} = \rho_h^{(s)}, \quad g_h^{n+1} = g_h^{(s)}, \tag{3.13}$$

where s is the total number of internal stages in the IMEX scheme. With the implicit treatment of stiff terms in (3.12) and the aforementioned assumption on $\mathcal{A}$ in (3.9), in the limit of $\varepsilon \to 0$, equation (3.12b) gives

$$v d_h(\rho_h^{(j)}, \psi) = s_{h,v}^{(1)}(\rho_h^{(j)}, g_h^{(j)}, \psi), \ \forall \psi \in U_h^k, \ \ \forall j = 1, \cdots, s. \tag{3.14}$$

The scheme being globally stiffly accurate further implies

$$v d_h(\rho_h^{n+1}, \psi) = s_{h,v}^{(1)}(\rho_h^{n+1}, g_h^{n+1}, \psi), \ \forall \psi \in U_h^k. \tag{3.15}$$

Therefore the scheme projects the numerical solutions, both from internal stages and at discrete times, to the limiting equilibrium when $\varepsilon \to 0$ as in equation (3.14) and (3.15) .

The second order globally stiffly accurate IMEX scheme used in this paper is the ARS(2, 2, 2) scheme [1] with a double Butcher Tableau

$$\begin{array}{c|ccc} 0 & 0 & 0 & 0 \\ \gamma & \gamma & 0 & 0 \\ 1 & \delta & 1-\delta & 0 \\ \hline & \delta & 1-\delta & 0 \end{array} \qquad \begin{array}{c|ccc} 0 & 0 & 0 & 0 \\ \gamma & 0 & \gamma & 0 \\ 1 & 0 & 1-\gamma & \gamma \\ \hline & 0 & 1-\gamma & \gamma \end{array}$$

where $\gamma = 1 - \frac{1}{\sqrt{2}}$ and $\delta = 1 - \frac{1}{2\gamma}$. The third order one is the ARS(4, 4, 3) scheme [1] with

$$\begin{array}{c|ccccc} 0 & 0 & 0 & 0 & 0 & 0 \\ 1/2 & 1/2 & 0 & 0 & 0 & 0 \\ 2/3 & 11/18 & 1/18 & 0 & 0 & 0 \\ 1/2 & 5/6 & -5/6 & 1/2 & 0 & 0 \\ 1 & 1/4 & 7/4 & 3/4 & -7/4 & 0 \\ \hline & 1/4 & 7/4 & 3/4 & -7/4 & 0 \end{array} \qquad \begin{array}{c|ccccc} 0 & 0 & 0 & 0 & 0 & 0 \\ 1/2 & 0 & 1/2 & 0 & 0 & 0 \\ 2/3 & 0 & 1/6 & 1/2 & 0 & 0 \\ 1/2 & 0 & -1/2 & 1/2 & 1/2 & 0 \\ 1 & 0 & 3/2 & -3/2 & 1/2 & 1/2 \\ \hline & 0 & 3/2 & -3/2 & 1/2 & 1/2 \end{array}$$

Remark 3.2. The DG methods with the first order IMEX temporal discretization can be implemented by explicitly solving (3.8a) for ρ^{n+1}, then solving for g^{n+1} from a block-diagonal system defined by (3.8b). The higher order globally stiffly accurate IMEX scheme can be implemented in a stage-by-stage fashion similar to the first order case.

Remark 3.3. The proposed DG-IMEX schemes can be straightforwardly extended to the multi-dimensional discrete-velocity kinetic problem

$$\varepsilon\partial_t f + \mathbf{v}\cdot\nabla_{\mathbf{x}} f = \frac{1}{\varepsilon}\mathcal{C}(f), \tag{3.16}$$

where $\mathbf{v} = (v_1, v_2, \ldots, v_d) \in \mathbb{R}^d$ with $v_l \in \{-1, 1\}$, $l = 1, \cdots d$ and $\mathbf{x} = (x_1, x_2, \ldots, x_d) \in \Omega_{\mathbf{x}} \subset \mathbb{R}^d$. The corresponding diffusive limit equations are the multi-dimensional heat equation, porous media equation, advection-diffusion equation, and viscous Burgers' equation. We refer to [20] for some of such examples.

3.3 Formal asymptotic analysis

In this subsection, we perform formal asymptotic analysis for the proposed DG-IMEX schemes as $\varepsilon \to 0$.

Proposition 3.4. Consider the DG-IMEX scheme (3.12)-(3.13) for the micro-macro formulation (2.4), with one choice of numerical fluxes in (3.5), a globally stiffly accurate IMEX scheme (3.9) with the aforementioned assumption on $\mathcal{A}$, consistent initial condition, and periodic boundary condition. Then, in the limit of $\varepsilon \to 0$,

($\mathcal{P}1$) the DG-IMEX scheme formally becomes: look for $\rho_h^{n+1}(\cdot)$, $g_h^{n+1}(\cdot, v) \in U_h^k$, satisfying (3.13), while the solutions from the internal stages $\rho_h^{(l)}(\cdot)$, $g_h^{(l)}(\cdot, v) \in U_h^k$ with $l = 1, \cdots, s$, satisfying

$$\left(\rho_h^{(l)}, \phi\right) = (\rho_h^n, \phi) - \Delta t \sum_{j=1}^{l-1} \tilde{a}_{lj} a_h(g_h^{(j)}, \phi), \tag{3.17a}$$

$$vd_h(\rho_h^{(l)}, \psi) = \begin{cases} (K(\rho_h^{(l)})^m g_h^{(l)}, \psi) & \text{for (2.7)} \\ (g_h^{(l)} - Av\rho_h^{(l)}, \psi) & \text{for (2.8)} \\ (g_h^{(l)} - Cv(\rho_h^{(l)})^2, \psi) & \text{for (2.11)} \end{cases} \tag{3.17b}$$

for any $\phi, \psi \in U_h^k$. This is a consistent scheme for the limiting equation with the corresponding numerical flux in (3.5) and the time discretization determined by the explicit part $\tilde{\mathcal{A}}$, $\tilde{b}$, $\tilde{c}$ in (3.9).

($\mathcal{P}2$) If one further denotes $q = \langle vg \rangle$ (so to their approximations), then the limiting scheme, (3.13) and (3.17), becomes a consistent local DG scheme for the heat and porous media equation, advection-diffusion equation, or viscous Burgers equation in its first order form as below,

$$\partial_t \rho + \partial_x q = 0, \quad q = \begin{cases} -\frac{1}{K(1-m)}\partial_x(\rho^{1-m}) \,, & \text{for (2.7)} \,, \\ A\rho - \partial_x \rho \,, & \text{for (2.8)} \,, \\ C\rho^2 - \partial_x \rho \,, & \text{for (2.11)} \,. \end{cases} \tag{3.18}$$

Proof. ($\mathcal{P}1$) can be obtained straightforwardly with the definition of $s_{h,v}^{(1)}(\rho_h, g_h, \psi)$ and the assumption on $\mathcal{A}$ in (3.9), as well as by formally taking $\varepsilon \to 0$ in (3.12)-(3.13). Note the time discretization comes directly from the explicit part of (3.9), and the numerical flux is carried over as well. To see that the limiting scheme gives a consistent discretization for the limiting

equation, one only needs to recall from Section 2.1 that the limiting equation, when written in the form of ρ and g, is given by

$$\partial_t \rho + \partial_x \langle vg \rangle = 0, \quad g = \begin{cases} -\frac{1}{K(1-m)} v \partial_x (\rho^{1-m}) , & \text{for (2.7)} , \\ Av\rho - v\partial_x \rho , & \text{for (2.8)} , \\ Cv\rho^2 - v\partial_x \rho , & \text{for (2.11)} . \end{cases} \tag{3.19}$$

Next we multiply equation (3.17b) with v, apply the $\langle \cdot \rangle$ operator, and denote $q = \langle vg \rangle$ (so to their approximations), then the limiting scheme becomes: look for $\rho_h^{(l)}, q_h^{(l)} \in U_h^k$ with $l = 1, \cdots, s$, such that

$$\left(\rho_h^{(l)}, \phi \right) = (\rho_h^n, \phi) - \Delta t \sum_{j=1}^{l-1} \tilde{a}_{lj} r_h(q_h^{(j)}, \phi), \quad \forall \phi \in U_h^k, \tag{3.20a}$$

$$d_h(\rho_h^{(l)}, \psi) = \begin{cases} (K(\rho_h^{(l)})^m q_h^{(l)}, \psi) & \text{for (2.7)} \\ (q_h^{(l)} - A\rho_h^{(l)}, \psi) & \text{for (2.8)} \\ (q_h^{(l)} - C(\rho_h^{(l)})^2, \psi) & \text{for (2.11)} \end{cases} \quad \forall \psi \in U_h^k, \tag{3.20b}$$

and $\rho_h^{n+1}, q_h^{n+1} \in U_h^k$ satisfying

$$\rho_h^{n+1} = \rho_h^{(s)}, \quad q_h^{n+1} = q_h^{(s)}. \tag{3.21}$$

Here d_h is given in (3.7c) and

$$r_h(q_h, \phi) = -\sum_i \int_{I_i} q_h \partial_x \phi dx - \sum_i \hat{q}_{h,i-\frac{1}{2}} [\phi]_{i-\frac{1}{2}}, \tag{3.22}$$

with $\hat{q}$ defined in the same fashion as $\langle vg \rangle$ (see (3.5)). This exactly gives a consistent local DG method for (3.18). □

Remark 3.5. (1) For the telegraph equation, the limit of the proposed scheme is closely related to the local DG method studied in [9], with the time discretization determined by the explicit part $\tilde{\mathcal{A}}, \tilde{b}, \tilde{c}$ in (3.9), for linear heat equation. It can be proved (see [9] for part of the analysis) that the semi-discrete local DG scheme for the heat equation with any of the alternating fluxes achieves an optimal $(k+1)^{th}$ order of accuracy, and the scheme with the central flux achieves a sub-optimal k^{th} order for odd k and an optimal $(k+1)^{th}$ order for even k, when piecewise polynomials of degree k are used as approximations. This is consistent with our numerical observations in Section 4.

(2) If the numerical flux in (3.5) is chosen based on the sign of A and C as discussed in section 3.1, then the convective term in the limiting equation will be discretized in an upwind fashion.

(3) In general, more rigorous analysis would be needed to show whether the limiting schemes, which are consistent with formal high order accuracy, are indeed stable and with good accuracy.

Remark 3.6. In Proposition 3.4, we assume consistent initial conditions, i.e. the initial conditions are well-prepared in the limit of $\varepsilon \to 0$. Such assumption is important to guarantee the high order convergence even when the time step size Δt is independent of ε; otherwise, one needs to resolve the initial layer by taking small time step size of $O(\varepsilon)$.

Remark 3.7. Instead of working with the micro-macro decomposition (2.4) to formulate numerical methods, one can also directly apply an upwind DG spatial discretization to the governing equation (2.1). Following a similar analysis as in [14], one can show that such discretizations coupled with a fully discrete time discretization will have AP property as long as the discrete space U_h^k is with $k \geq 1$. (When $k = 0$, the numerical dissipation of such scheme is of $O(\frac{\Delta x}{\varepsilon})$, thus the scheme is of little use when $\varepsilon \ll \Delta x$.) In this case, the limiting scheme as $\varepsilon \to 0$ approximates the density ρ with *continuous* piecewise polynomial functions. On the other hand, such methods are computationally more expensive than our proposed methods due to the fully implicit treatments in time.

4 Numerical Examples

In this section, we will demonstrate the performance of the proposed schemes by applying them to several numerical examples. Two kinds of fluxes in (3.5) will be used: alternating and central. For alternating fluxes, without specifying, we would use (3.5a) which is referred to as the "left-right flux". Likewise, (3.5b) will be called the "right-left flux". Our scheme is denoted as "DG(k+1)-IMEX(k+1)" if piecewise polynomials of degree at most k are used in the discrete space (3.1) together with the $(k+1)^{th}$ order IMEX scheme in time, for $k = 0, 1, 2$. The simulation is carried out up to the final time T on uniform meshes with totally N elements. The time step Δt is determined by

$$\Delta t = C_{hyper}\varepsilon\Delta x + C_{diff}\Delta x^2.$$

That is, $\Delta t = O(\varepsilon\Delta x)$ in the rarefied (convective) regime where $\varepsilon = O(1)$, and $\Delta t = O(\Delta x^2)$ in the parabolic (diffusive) regime where $\varepsilon << 1$. We take $C_{hyper} = 0.5$ and $C_{diff} = 0.25$ for DG1-IMEX1, and this is based on a uniform stability analysis of the method for the telegraph equation [16]. As for DG(k+1)-IMEX(k+1) with $k > 0$, C_{hyper} and C_{diff} are chosen based on the numerical simulations with $\varepsilon = O(1), 10^{-2}, 10^{-6}$. In particular, we take $C_{hyper} = 0.5$ and $C_{diff} = 0.01$ for DG2-IMEX2, and $C_{hyper} = 0.25$ and $C_{diff} = 0.006$ for DG3-IMEX3.

4.1 Telegraph equation

Consider (2.7) with $m = 0$ and $K = 1$. We test the accuracy for our scheme with the following exact solution

$$\begin{cases} \rho(x,t) = \frac{1}{r}\exp(rt)\sin(x), \quad r = \frac{-2}{1+\sqrt{1-4\varepsilon^2}}, \\ j(x,t) = \exp(rt)\cos(x) \end{cases} \tag{4.1}$$

on the domain $[-\pi, \pi]$ with periodic boundary conditions. In Tables 4.1-4.3, we show the errors and orders of accuracy with $\varepsilon = 0.5, 10^{-2}, 10^{-6}$ for DG(k+1)-IMEX(k+1), $k = 0, 1, 2$, respectively. Alternating left-right flux is used and $T = 1$. For all three εs, a uniform $(k+1)^{th}$ order of convergence is observed for DG(k+1)-IMEX(k+1). We further present in Tables 4.4-4.6 the results from DG(k+1)-IMEX(k+1) using the central flux. For all three εs, a uniform $(k+1)^{th}$ order for even k and k^{th} order for odd k is observed.

Next we consider a Riemann problem for the telegraph equation, with initial conditions

$$\begin{cases} \rho(x,0) = \rho_L = 2.0, \quad j(x,0) = j_L = 0.0, \qquad -1 < x < 0, \\ \rho(x,0) = \rho_R = 1.0, \quad j(x,0) = j_R = 0.0, \qquad 0 < x < 1, \end{cases} \tag{4.2}$$

Table 4.1: L^1 errors and orders of ρ and j for the telegraph equation with the exact solution (4.1), $T = 1.0$, DG1-IMEX1 with left-right flux.

	N	L^1 error of ρ	order	L^1 error of j	order
$\varepsilon = 0.5$	10	6.04E-02	–	7.46E-02	–
	20	2.19E-02	1.46	3.38E-02	1.14
	40	9.20E-03	1.25	1.60E-02	1.08
	80	4.19E-03	1.14	7.81E-03	1.03
	160	2.00E-03	1.07	3.86E-03	1.02
$\varepsilon = 10^{-2}$	10	3.79E-02	–	8.05E-02	–
	20	1.78E-02	1.09	3.77E-02	1.09
	40	8.79E-03	1.02	1.85E-02	1.03
	80	4.36E-03	1.01	9.22E-03	1.01
	160	2.17E-03	1.01	4.60E-03	1.00
$\varepsilon = 10^{-6}$	10	3.79E-02	–	8.03E-02	–
	20	1.79E-02	1.08	3.76E-02	1.09
	40	8.82E-03	1.02	1.85E-02	1.02
	80	4.38E-03	1.01	9.21E-03	1.01
	160	2.18E-03	1.01	4.60E-03	1.00

Table 4.2: L^1 errors and orders of ρ and j for the telegraph equation with the exact solution (4.1), $T = 1.0$, DG2-IMEX2 with left-right flux.

	N	L^1 error of ρ	order	L^1 error of j	order
$\varepsilon = 0.5$	10	1.35E-03	–	2.36E-03	–
	20	3.00E-04	2.17	4.90E-04	2.27
	40	7.23E-05	2.05	1.14E-04	2.10
	80	1.79E-05	2.01	2.76E-05	2.04
	160	4.46E-06	2.01	6.82E-06	2.02
$\varepsilon = 10^{-2}$	10	4.83E-03	–	4.94E-03	–
	20	1.19E-03	2.02	1.19E-03	2.06
	40	2.96E-04	2.01	2.97E-04	2.00
	80	7.40E-05	2.00	7.40E-05	2.00
	160	1.85E-05	2.00	1.85E-05	2.00
$\varepsilon = 10^{-6}$	10	4.82E-03	–	4.93E-03	–
	20	1.19E-03	2.02	1.18E-03	2.06
	40	2.96E-04	2.00	2.96E-04	2.00
	80	7.40E-05	2.00	7.40E-05	2.00
	160	1.85E-05	2.00	1.85E-05	2.00

Table 4.3: L^1 errors and orders of ρ and j for the telegraph equation with the exact solution (4.1), $T = 1.0$, DG3-IMEX3 with left-right flux.

	N	L^1 error of ρ	order	L^1 error of j	order
$\varepsilon = 0.5$	10	6.33E-05	–	9.48E-05	–
	20	7.54E-06	3.07	1.15E-05	3.04
	40	9.31E-07	3.02	1.44E-06	3.00
	80	1.16E-07	3.01	1.80E-07	3.00
	160	1.44E-08	3.00	2.24E-08	3.00
$\varepsilon = 10^{-2}$	10	2.53E-04	–	2.46E-04	–
	20	3.11E-05	3.03	3.11E-05	2.98
	40	3.89E-06	3.00	3.89E-06	3.00
	80	4.87E-07	3.00	4.87E-07	3.00
	160	6.09E-08	3.00	6.09E-08	3.00
$\varepsilon = 10^{-6}$	10	2.53E-04	–	2.46E-04	–
	20	3.11E-05	3.03	3.11E-05	2.98
	40	3.89E-06	3.00	3.89E-06	3.00
	80	4.87E-07	3.00	4.87E-07	3.00
	160	6.09E-08	3.00	6.09E-08	3.00

Table 4.4: L^1 errors and orders of ρ and j for the telegraph equation with the exact solution (4.1), $T = 1.0$, DG1-IMEX1 with central flux.

	N	L^1 error of ρ	order	L^1 error of j	order
$\varepsilon = 0.5$	10	2.49E-02	–	3.80E-02	–
	20	9.80E-03	1.34	1.74E-02	1.13
	40	4.42E-03	1.15	8.17E-03	1.09
	80	2.07E-03	1.10	3.99E-03	1.03
	160	1.00E-03	1.04	1.97E-03	1.02
$\varepsilon = 10^{-2}$	10	4.14E-02	–	3.46E-02	–
	20	1.89E-02	1.13	1.74E-02	0.99
	40	9.04E-03	1.07	8.71E-03	1.00
	80	4.43E-03	1.03	4.36E-03	1.00
	160	2.20E-03	1.01	2.18E-03	1.00
$\varepsilon = 10^{-6}$	10	4.12E-02	–	3.46E-02	–
	20	1.89E-02	1.13	1.74E-02	0.99
	40	9.01E-03	1.07	8.69E-03	1.00
	80	4.42E-03	1.03	4.34E-03	1.00
	160	2.19E-03	1.01	2.17E-03	1.00

Table 4.5: L^1 errors and orders of ρ and j for the telegraph equation with the exact solution (4.1), $T = 1.0$, DG2-IMEX2 with central flux.

	N	L^1 error of ρ	order	L^1 error of j	order
$\varepsilon = 0.5$	10	1.31E-02	–	8.93E-03	–
	20	1.06E-02	0.30	3.64E-03	1.29
	40	7.20E-03	0.56	1.25E-03	1.54
	80	4.26E-03	0.76	3.74E-04	1.74
	160	2.33E-03	0.87	1.03E-04	1.86
$\varepsilon = 10^{-2}$	10	1.02E-02	–	1.01E-02	–
	20	4.51E-03	1.18	4.78E-03	1.09
	40	1.95E-03	1.21	2.37E-03	1.01
	80	7.58E-04	1.37	1.24E-03	0.94
	160	1.53E-04	2.31	6.90E-04	0.85
$\varepsilon = 10^{-6}$	10	1.06E-02	–	1.00E-02	–
	20	4.83E-03	1.13	4.66E-03	1.10
	40	2.29E-03	1.08	2.25E-03	1.05
	80	1.11E-03	1.04	1.11E-03	1.03
	160	5.50E-04	1.02	5.48E-04	1.01

Table 4.6: L^1 errors and orders of ρ and j for the telegraph equation with the exact solution (4.1), $T = 1.0$, DG3-IMEX3 with central flux.

	N	L^1 error of ρ	order	L^1 error of j	order
$\varepsilon = 0.5$	10	6.56E-05	–	7.13E-05	–
	20	7.10E-06	3.21	7.76E-06	3.20
	40	8.14E-07	3.13	9.81E-07	2.98
	80	9.49E-08	3.10	1.11E-07	3.14
	160	1.24E-08	2.93	1.51E-08	2.88
$\varepsilon = 10^{-2}$	10	1.77E-04	–	1.76E-04	–
	20	2.05E-05	3.11	2.04E-05	3.11
	40	2.49E-06	3.04	2.48E-06	3.04
	80	3.07E-07	3.02	3.05E-07	3.02
	160	3.81E-08	3.01	3.79E-08	3.01
$\varepsilon = 10^{-6}$	10	1.76E-04	–	1.76E-04	–
	20	2.04E-05	3.11	2.04E-05	3.11
	40	2.48E-06	3.04	2.48E-06	3.04
	80	3.05E-07	3.02	3.05E-07	3.02
	160	3.79E-08	3.01	3.79E-08	3.01

and inflow and outflow boundary conditions on the computational domain $[-1, 1]$. We depict in Figure 4.1 the numerical solutions of ρ and j from DG(k+1)-IMEX(k+1), $k = 0, 1, 2$ in the rarefied regime ($\varepsilon = 0.7$) at $T = 0.25$ and in the parabolic regime ($\varepsilon = 10^{-6}$) at $T = 0.04$. Alternating left-right flux and central flux are used. The mesh size is $\Delta x = 0.05$. The reference solutions are obtained using DG3-IMEX3 with the corresponding numerical flux on a more refined grid of $\Delta x = 0.004$. One can see that the higher order scheme (DG3-IMEX3) has much better resolution than the lower order one (DG1-IMEX1). Compared with the results in [20], the high order results can also catch the shock speed well for such a coarse mesh. Small oscillations are observed for our scheme with any of the numerical fluxes in the rarefied regime, even for DG1-IMEX1, due to the dispersive error of the scheme. DG3-IMEX3 demonstrates better control over the numerical oscillations than DG2-IMEX2.

For this example, one can see that the scheme with alternating fluxes has better order of accuracy, see especially the case with odd k, than that using central flux when the solutions are smooth. For Riemann problem, the scheme with alternating flux also performs better with smaller numerical oscillation. On the other hand, the scheme using central flux can be more flexible for some other problems, see for example those in Section 4.4.

The remaining two examples in this subsection concern the telegraph equation with a variable $\varepsilon(x)$:

$$\varepsilon(x) = \varepsilon_M\Big(\varepsilon_0 + \frac{1}{2}(\tanh(1 - 12x) + \tanh(1 + 12x))\Big). \tag{4.3}$$

In order to conveniently deal with the multi-scale nature of $\varepsilon(x)$, the DG scheme is implemented in the nodal fashion [15]. That is, we use the Lagrangian basis functions at $k + 1$ Gaussian points to represent a polynomial space of degree k. We first test the accuracy for a problem with the following initial conditions

$$\begin{cases} \rho(x, 0) = \frac{1}{r}\sin(x), \quad r = \frac{-2}{1+\sqrt{1-4\varepsilon(x)^2}}, \\ j(x, 0) = \cos(x) \end{cases} \tag{4.4}$$

on the domain $[-\pi, \pi]$ and periodic boundary conditions. Since the exact solution is not available, the L^1 errors are computed as the difference of the numerical solutions on two consecutive meshes,

$$L^1 \text{ error } (h) = \frac{1}{2\pi}\sum_i \int_{I_i} |u_h - u_{h/2}| dx \ , \tag{4.5}$$

where u_h is the numerical solution when the mesh size is h, I_i is an element from the finer mesh with the mesh size $h/2$, and u is ρ or j. The 5-point Gaussian quadrature rule is used to approximate the integral in (4.5). The convergence order is computed by

$$\text{order } = \frac{\log\left(L^1 \text{ error } (h)/L^1 \text{ error } (h/2)\right)}{\log 2} \tag{4.6}$$

In Tables 4.7, we show the errors and orders of accuracy for DG(k+1)-IMEX(k+1), $k = 0, 1, 2$, respectively. Alternating left-right flux is used and $T = 0.0001$. We take $\varepsilon_M = 0.5$ and $\varepsilon_0 = 10^{-6}$. A uniform $(k + 1)^{th}$ order of convergence is observed for DG(k+1)-IMEX(k+1).

The second example with the variable $\varepsilon(x)$ in (4.3) starts with discontinuous initial conditions

$$\begin{cases} \rho(x, 0) = \rho_L = 2.0, \quad j(x, 0) = j_L = 0.0, \qquad -1 < x < 0, \\ \rho(x, 0) = \rho_R = 1.0, \quad j(x, 0) = j_R = 0.0, \qquad 0 < x < 1, \end{cases} \tag{4.7}$$

Table 4.7: L^1 errors and orders of ρ and j for the telegraph equation with the initial condition (4.4), $T = 0.0001$, alternating left-right flux.

	N	L^1 error of ρ	order	L^1 error of j	order
DG1-IMEX1	80	1.25E-02	–	1.29E-02	–
	160	6.25E-03	1.00	6.40E-03	1.01
	320	3.12E-03	1.00	3.18E-03	1.01
DG2-IMEX2	80	1.71E-04	–	4.33E-03	–
	160	4.79E-05	1.83	5.71E-04	2.92
	320	1.25E-05	1.93	1.12E-04	2.36
DG3-IMEX3	80	4.32E-06	–	2.01E-04	–
	160	8.99E-07	2.26	2.24E-05	3.17
	320	1.38E-07	2.70	2.58E-06	3.12

together with inflow and outflow boundary conditions on the computational domain $[-1, 1]$. We depict in Figure 4.2 the numerical solutions of ρ and $\varepsilon(x)j$ from DG(k+1)-IMEX(k+1), $k = 0, 1, 2$ at $T = 0.06$. Alternating left-right flux is used. The mesh size is $\Delta x = 0.005$. We take $\varepsilon_M = 0.7$ and $\varepsilon_0 = 10^{-2}$. The reference solutions are obtained by using DG1 with the explicit Euler forward time discretization on a much refined grid of $\Delta x = 5 \times 10^{-5}$. One can also see that the higher order scheme (DG3-IMEX3) has much better resolution than the lower order one (DG1-IMEX1).

4.2 Advection-diffusion equation

Consider (2.8) with $A = 1$. As $\varepsilon \to 0$, this leads to the classical advection-diffusion equation (2.9) as the limiting equation. By taking into account the convection term with $A = 1$, we only use the left-right flux throughout this subsection.

Note that the limiting advection-diffusion equation (2.9) with $A = 1$ admits the following exact solution

$$\rho(x, t) = e^{-t} \sin(x - t), \qquad j(x, t) = e^{-t}(\sin(x - t) - \cos(x - t)), \tag{4.8}$$

on the domain $[-\pi, \pi]$ with periodic boundary conditions. We start with the initial conditions (4.8) at $t = 0$, and implement our scheme with $\varepsilon = 10^{-6}$ up to $T = 0.1$. The numerical results are compared with (4.8), with errors and convergence orders reported in Table 4.8. One can observe $(k + 1)^{th}$ order of accuracy for DG(k+1)-IMEX(k+1), $k = 0, 1, 2$.

Next we consider a Riemann problem, with the initial conditions given as

$$\begin{cases} \rho(x, 0) = \rho_L = 4.0, \quad j(x, 0) = j_L = 0.0, & -10 < x < 0, \\ \rho(x, 0) = \rho_R = 2.0, \quad j(x, 0) = j_R = 0.0, & 0 < x < 10, \end{cases} \tag{4.9}$$

and inflow and outflow boundary conditions. The exact solution for the limiting advection-diffusion equation (2.9) is

$$\rho(x, t) = \frac{1}{2}(\rho_L + \rho_R) + \frac{1}{2}(\rho_L - \rho_R) erf(\frac{(t - x)}{2\sqrt{t}}) \tag{4.10}$$

where erf denotes the error function. We compute the numerical solutions of DG(k+1)-IMEX(k+1) for $k = 0, 1, 2$ with mesh size $\Delta x = 0.5$ on the domain $[-10, 10]$ up to $T = 3.0$.

Table 4.8: L^1 errors and orders of ρ and j for the advection-diffusion equation for $\varepsilon = 10^{-6}$, with the numerical solutions compared with the exact solutions (4.8) to the limiting equation, $T = 0.1$, left-right flux.

	N	L^1 error of ρ	order	L^1 error of j	order
DG1-IMEX1	10	9.41E-02	–	2.03E-01	–
	20	4.62E-02	1.03	9.94E-02	1.03
	40	2.30E-02	1.01	4.98E-02	1.00
	80	1.15E-02	1.00	2.50E-02	0.99
	160	5.74E-03	1.00	1.25E-02	1.00
DG2-IMEX2	10	1.03E-02	–	1.67E-02	–
	20	2.71E-03	1.92	4.10E-03	2.02
	40	7.01E-04	1.95	1.03E-03	2.00
	80	1.79E-04	1.97	2.57E-04	2.00
	160	4.51E-05	1.99	6.43E-05	2.00
DG3-IMEX3	10	6.05E-04	–	8.57E-04	–
	20	7.62E-05	2.99	1.08E-04	2.98
	40	9.56E-06	3.00	1.36E-05	3.00
	80	1.20E-06	3.00	1.69E-06	3.00
	160	1.50E-07	3.00	2.12E-07	3.00

For $\varepsilon = 0.5$, we compare the numerical solution ρ and the reference solution obtained by DG3-IMEX3 on a much fine mesh ($\Delta x = 0.04$) in Figure 4.3 (left). On the right of Figure 4.3, we plot the numerical solution from the scheme with $\varepsilon = 10^{-6}$, and the analytical solution (4.10). In both regimes, numerical solutions match the reference or exact solutions very well. The profiles for j are similar to that for ρ, and they are omitted to save space.

4.3 Viscous Burgers' equation

Consider (2.11) with $C = 1/2$. The initial conditions are chosen to be two local Maxwellian

$$\rho(x,0) = \begin{cases} \rho_L = 2.0, & -10 < x < 0, \\ \rho_R = 1.0, & 0 < x < 10, \end{cases} \tag{4.11}$$

with $j = \rho^2/(1+\sqrt{1+\rho^2\varepsilon^2})$. For this problem, we show in Figure 4.4 the numerical solutions ρ and j of DG(k+1)-IMEX(k+1), $k = 0, 1, 2$ using the left-right flux in the rarefied regime ($\varepsilon = 0.4$) and in the parabolic regime ($\varepsilon = 10^{-6}$) with $\Delta x = 0.25$, which are compared with the reference solutions obtained by DG3-IMEX3 with $\Delta x = 0.04$. Numerical solutions are in very good agreement with the reference solutions.

For this nonlinear example, an exact smooth shock wave solution was given by Ruijgrok and Wu in [32]. We choose the similar boundary condition as (4.11)

$$\lim_{x\to+\infty} \rho = \rho^+ = 2.0, \qquad \lim_{x\to-\infty} \rho = \rho^- = 1.0, \tag{4.12}$$

with $j^\pm = (\rho^\pm)^2/(1+\sqrt{1+(\rho^\pm)^2\varepsilon^2})$. Let

$$u^\pm = \rho^\pm + \varepsilon j^\pm, \quad v^\pm = \rho^\pm - \varepsilon j^\pm. \tag{4.13}$$

Table 4.9: L^1 errors and orders of ρ and j for the viscous Burgers' equation with the exact solution (4.12)-(4.14), $T = 1.0$, DG1-IMEX1 with left-right flux.

	N	L^1 error of ρ	order	L^1 error of j	order
$\varepsilon = 0.5$	10	2.98E-02	–	3.46E-02	–
	20	1.39E-02	1.11	1.57E-02	1.14
	40	6.48E-03	1.10	7.92E-03	0.98
	80	3.25E-03	0.99	3.93E-03	1.01
	160	1.66E-03	0.97	1.89E-03	1.06
$\varepsilon = 10^{-2}$	10	3.08E-02	–	4.52E-02	–
	20	1.41E-02	1.13	2.00E-02	1.18
	40	6.38E-03	1.14	9.13E-03	1.13
	80	3.39E-03	0.91	4.68E-03	0.96
	160	1.76E-03	0.94	2.42E-03	0.95
$\varepsilon = 10^{-6}$	10	3.08E-02	–	4.52E-02	–
	20	1.41E-02	1.13	2.00E-02	1.18
	40	6.38E-03	1.14	9.14E-03	1.13
	80	3.39E-03	0.91	4.68E-03	0.97
	160	1.76E-03	0.94	2.42E-03	0.95

The distribution function $u(x,t)$ and $v(x,t)$ are given by

$$u(x,t) = \frac{u^+ + u^- e^{-(\xi-\xi_0)/X_0}}{1+e^{-(\xi-\xi_0)/X_0}}, \quad v(x,t) = \frac{v^+ + v^- e^{-(\xi-\xi_0)/X_0}}{1+e^{-(\xi-\xi_0)/X_0}}$$

where $\xi = (x - wt/\varepsilon)/2$ and let $\xi_0 = 0$. The width X_0 and the velocity w of the shock wave are

$$X_0 = \frac{1+w}{u^- - u^+} = \frac{1-w}{v^- - v^+}, \quad w = \frac{u^- - u^+ - v^- + v^+}{u^- - u^+ + v^- - v^+}.$$

With above, the exact solutions $\rho(x,t)$ and $j(x,t)$ are given by

$$\rho(x,t) = \frac{u(x,t)+v(x,t)}{2}, \quad j(x,t) = \frac{u(x,t)-v(x,t)}{2\varepsilon} \tag{4.14}$$

The computational domain is taken to be $[-40, 40]$ with inflow and outflow boundary conditions. Starting from the smooth initial condition at $t = 0$, we compute up to $T = 1$ for $\varepsilon = 0.5, 10^{-2}, 10^{-6}$. The numerical results by DG(k+1)-IMEX(k+1) with the left-right alternating flux are presented in Tables 4.9-4.11 for $k = 0, 1, 2$, respectively, and $(k+1)^{th}$ order is observed. In Tables 4.12-4.14, $(k+1)^{th}$ order is observed for even k and k^{th} order for odd k when DG(k+1)-IMEX(k+1) are combined with the central flux (3.5c).

4.4 Porous media equation

Consider (2.7) with $m = -1$ and $K = 1/2$, and the limiting equation is the porous media equation. We compare the numerical solutions of DG(k+1)-IMEX(k+1), $k = 0, 1, 2$ for $\varepsilon = 10^{-6}$ with the exact Barenblatt solution of the limiting porous media equation,

$$\begin{cases} \rho(x,t) = \frac{1}{R(t)}\left[1 - \left(\frac{x}{R(t)}\right)^2\right], \quad j(x,t) = \rho(x,t)\frac{4x}{R(t)^3}, \quad |x| < R(t), \\ \rho(x,t) = 0, \quad j(x,t) = 0, \quad |x| > R(t), \end{cases} \tag{4.15}$$

Table 4.10: L^1 errors and orders of ρ and j for the viscous Burgers' equation with the exact solution (4.12)-(4.14), $T = 1.0$, DG2-IMEX2 with left-right flux.

	N	L^1 error of ρ	order	L^1 error of j	order
$\varepsilon = 0.5$	10	5.78E-03	–	7.07E-03	–
	20	1.84E-03	1.65	2.48E-03	1.51
	40	4.27E-04	2.10	6.78E-04	1.87
	80	9.80E-05	2.13	1.50E-04	2.18
	160	2.50E-05	1.97	4.72E-05	1.67
$\varepsilon = 10^{-2}$	10	6.26E-03	–	9.20E-03	–
	20	1.85E-03	1.76	3.57E-03	1.36
	40	4.27E-04	2.11	9.83E-04	1.86
	80	1.22E-04	1.80	2.43E-04	2.02
	160	3.34E-05	1.87	6.03E-05	2.01
$\varepsilon = 10^{-6}$	10	6.24E-03	–	9.25E-03	–
	20	1.85E-03	1.76	3.62E-03	1.35
	40	4.29E-04	2.11	9.84E-04	1.88
	80	1.23E-04	1.80	2.43E-04	2.02
	160	3.37E-05	1.87	6.04E-05	2.01

Table 4.11: L^1 errors and orders of ρ and j for the viscous Burgers' equation with the exact solution (4.12)-(4.14), $T = 1.0$, DG3-IMEX3 with left-right flux.

	N	L^1 error of ρ	order	L^1 error of j	order
$\varepsilon = 0.5$	10	2.51E-03	–	5.39E-03	–
	20	2.48E-04	3.34	4.06E-04	3.73
	40	2.74E-05	3.18	4.70E-05	3.11
	80	3.54E-06	2.96	6.11E-06	2.94
	160	4.56E-07	2.96	7.66E-07	3.00
$\varepsilon = 10^{-2}$	10	2.13E-03	–	3.92E-03	–
	20	2.26E-04	3.24	4.26E-04	3.20
	40	3.30E-05	2.77	5.93E-05	2.84
	80	4.71E-06	2.81	7.66E-06	2.95
	160	6.23E-07	2.92	9.68E-07	2.98
$\varepsilon = 10^{-6}$	10	2.13E-03	–	4.01E-03	–
	20	2.26E-04	3.24	4.27E-04	3.23
	40	3.33E-05	2.76	5.97E-05	2.84
	80	4.76E-06	2.81	7.78E-06	2.94
	160	6.29E-07	2.92	9.94E-07	2.97

Table 4.12: L^1 errors and orders of ρ and j for the viscous Burgers' equation with the exact solution (4.12)-(4.14), $T = 1.0$, DG1-IMEX1 with central flux.

	N	L^1 error of ρ	order	L^1 error of j	order
$\varepsilon = 0.5$	10	2.89E-02	–	3.71E-02	–
	20	1.30E-02	1.16	1.61E-02	1.20
	40	6.48E-03	1.00	8.51E-03	0.92
	80	3.18E-03	1.03	4.06E-03	1.07
	160	1.55E-03	1.03	1.93E-03	1.08
$\varepsilon = 10^{-2}$	10	3.02E-02	–	5.08E-02	–
	20	1.33E-02	1.18	2.17E-02	1.23
	40	7.07E-03	0.91	1.11E-02	0.97
	80	3.18E-03	1.15	4.80E-03	1.21
	160	1.53E-03	1.05	2.31E-03	1.06
$\varepsilon = 10^{-6}$	10	3.02E-02	–	5.08E-02	–
	20	1.33E-02	1.18	2.17E-02	1.23
	40	7.07E-03	0.91	1.11E-02	0.97
	80	3.18E-03	1.15	4.81E-03	1.21
	160	1.53E-03	1.05	2.31E-03	1.06

Table 4.13: L^1 errors and orders of ρ and j for the viscous Burgers' equation with the exact solution (4.12)-(4.14), $T = 1.0$, DG2-IMEX2 with central flux.

	N	L^1 error of ρ	order	L^1 error of j	order
$\varepsilon = 0.5$	10	6.98E-03	–	7.74E-03	–
	20	3.46E-03	1.01	3.33E-03	1.21
	40	1.66E-03	1.06	1.25E-03	1.41
	80	8.23E-04	1.01	4.48E-04	1.48
	160	4.17E-04	0.98	1.43E-04	1.65
$\varepsilon = 10^{-2}$	10	8.25E-03	–	1.50E-02	–
	20	3.65E-03	1.18	7.21E-03	1.06
	40	1.74E-03	1.07	3.49E-03	1.05
	80	8.50E-04	1.04	1.68E-03	1.06
	160	4.23E-04	1.01	7.96E-04	1.07
$\varepsilon = 10^{-6}$	10	8.23E-03	–	1.51E-02	–
	20	3.65E-03	1.17	7.29E-03	1.05
	40	1.74E-03	1.07	3.57E-03	1.03
	80	8.42E-04	1.05	1.75E-03	1.03
	160	4.14E-04	1.02	8.63E-04	1.02

Table 4.14: L^1 errors and orders of ρ and j for the viscous Burgers' equation with the exact solution (4.12)-(4.14), $T = 1.0$, DG3-IMEX3 with central flux.

	N	L^1 error of ρ	order	L^1 error of j	order
$\varepsilon = 0.5$	10	3.98E-03	–	4.80E-03	–
	20	5.97E-04	2.74	6.66E-04	2.85
	40	4.11E-05	3.86	4.20E-05	3.99
	80	4.20E-06	3.29	4.29E-06	3.29
	160	5.08E-07	3.05	4.95E-07	3.12
$\varepsilon = 10^{-2}$	10	4.92E-03	–	1.05E-02	–
	20	7.21E-04	2.77	1.52E-03	2.79
	40	3.85E-05	4.23	6.54E-05	4.54
	80	3.55E-06	3.44	5.34E-06	3.61
	160	4.20E-07	3.08	6.29E-07	3.08
$\varepsilon = 10^{-6}$	10	4.95E-03	–	1.06E-02	–
	20	7.26E-04	2.77	1.56E-03	2.77
	40	3.86E-05	4.23	6.64E-05	4.55
	80	3.55E-06	3.44	5.49E-06	3.60
	160	4.20E-07	3.08	6.56E-07	3.06

where $R(t) = [12(t+1)]^{1/3}$, $t \geq 0$.

For this example, there are two implementation issues one needs to pay attention to. First, to avoid being divided by zero in the collision term (note ρ is or is close to 0 in part of the computational domain), the DG scheme is implemented in the nodal fashion [15]. Specifically, we use the Lagrangian basis functions at $k+1$ Gaussian points to represent a polynomial space of degree k. Secondly, when alternating fluxes are used, to ensure the interface of $\rho = 0$ propagating outward in time, we choose the right-left flux in the left half of the domain to ensure the left interface of $\rho = 0$ is propagating to the left, and the left-right flux in the right half of the domain to ensure the right interface of $\rho = 0$ is propagating to the right. With this strategy, in the transition interval which uses the left-right flux as its flux on the left boundary, and right-left flux as its flux on the right boundary, the scheme loses one order accuracy. Because of this, the first order scheme becomes inconsistent and the corresponding result is not presented here. In Figure 4.5, we show numerical results of DG(k+1)-IMEX(k+1) at $T = 3.0$ with $\Delta x = 0.5$: with the left ones using alternating fluxes for $k = 1, 2$, and the right ones using the central flux for $k = 0, 1, 2$. The numerical solutions very well capture the exact solution of the limiting equation. Moreover, higher order schemes (i.e. DG3-IMEX3) demonstrate better resolution. For this example, when ε is of order 1, i.e., $\varepsilon = 0.5$, if we choose the initial condition (4.2), the numerical results are very similar to the ones in Figure 4.1, and the results are omitted here due to similarity.

5 One-group transport equation in slab geometry

In this section, we will extend the proposed numerical methods for discrete-velocity kinetic models to solve the continuous-velocity one-group transport equation in slab geometry. This

continuous-velocity model in one dimension [24] can be written as

$$\varepsilon\partial_t f + v\partial_x f = \frac{\sigma_S}{\varepsilon}(\langle f\rangle - f) - \varepsilon\sigma_A f + \varepsilon G, \tag{5.16}$$

where $\sigma_S(\langle f\rangle - f)$ is the scattering operator, and $-\varepsilon\sigma_A f + G$ is the "source" term. σ_S and σ_A are scattering and absorbing coefficients, respectively, which might depend on x. Here the velocity is the set of cosine angles with $v \in [-1,1]$, and $\langle f\rangle := \frac{1}{2}\int_{-1}^{1} f dv$ with dv being the standard Lebesgue measure on $[-1,1]$. The corresponding micro-macro formulation of (5.16) is

$$\partial_t \rho + \partial_x\langle vg\rangle = -\sigma_A\rho + G, \tag{5.17a}$$

$$\partial_t g + \frac{1}{\varepsilon}(\mathbf{I}-\Pi)(v\partial_x g) + \frac{1}{\varepsilon^2}v\partial_x\rho = -\frac{\sigma_S}{\varepsilon^2}g - \sigma_A g. \tag{5.17b}$$

Dirichlet boundary conditions are considered with

$$f(x_L, v, t) = f_L(v,t), \quad v \geq 0, \qquad \text{and} \qquad f(x_R, v, t) = f_R(v,t), \quad v < 0, \tag{5.18}$$

where x_L and x_R are left and right boundary points. In the limit of $\varepsilon \to 0$, the equation (5.16) will lead to a diffusion equation [24].

Numerically, in the v direction, we discretize $[-1,1]$ with N_v Gaussian quadrature points. This will result in a discrete-velocity system, and $\langle\cdot\rangle$ should be understood as its naturally induced discrete version. The DG-IMEX schemes for (5.17) can be defined in a similar fashion as those described in Section 3, and the scheme formulations are omitted here for brevity. To implement the Dirichlet boundary conditions, we propose the following procedure for DG-IMEX1 scheme at the left boundary, assuming that the central fluxes as specified in (3.5c) are used. Such procedure is based on the inflow and outflow principle and can be directly extended to the right boundary treatment, other type of fluxes, and higher order IMEX time discretizations. We let $I_1 = [x_{\frac{1}{2}}, x_{\frac{3}{2}}]$ be the left-most computational cell with $x_L = x_{\frac{1}{2}}$ and let ρ_L^n and $g_{L,v}^n$ approximate $\rho(x_L,t)$ and $g(x_L,v,t)$ at time $t = t^n$. We assume ρ_h^n, g_h^n, ρ_L^n and g_L^n are already known at time step n.

1.) First, ρ_h^{n+1} can be explicitly updated from (5.17a), with the numerical flux for $\langle vg\rangle$ at the left boundary at t^n being $\widehat{\langle vg_h\rangle}_{\frac{1}{2}} = \frac{1}{2}\left(g_{L,v}^n + g_h^n(x_{\frac{1}{2}}^+, v)\right)$.

2.) Update g_h^{n+1}. However, in cell I_1, we need the numerical flux

$$\hat{\rho}_{\frac{1}{2}} = \frac{1}{2}\left(\rho_L^{n+1} + \rho_h^{n+1}(x_{\frac{1}{2}}^+)\right) \tag{5.19}$$

based on (3.5c) at the left boundary at t^{n+1}. $\rho_h^{n+1}(x_{\frac{1}{2}}^+)$ is already known from the previous step 1.). So g_h^{n+1} in the cell I_1 can be expressed as a (linear) function of ρ_L^{n+1} via an DG-IMEX1 discretization of (5.17b), i.e. $g_h^{n+1} = g_h^{n+1}(\rho_L^{n+1})$; such dependence is from the numerical flux at the boundary (5.19).

3.) Solve ρ_L^{n+1} and $g_{L,v}^{n+1}$ from the given boundary and interior data via inflow and outflow numerical boundary conditions:

$$\rho_L^{n+1} + \varepsilon g_{L,v}^{n+1} = f_L(v, t^{n+1}), \quad v \geq 0 \quad \text{(inflow)}, \tag{5.20a}$$

$$\rho_L^{n+1} + \varepsilon g_{L,v}^{n+1} = \rho_h^{n+1}(x_{\frac{1}{2}}^+) + \varepsilon g_h^{n+1}(x_{\frac{1}{2}}^+, v), \quad v < 0 \quad \text{(outflow)}, \tag{5.20b}$$

$$\langle g_{L,v}^{n+1}\rangle = 0. \tag{5.20c}$$

Notice that ρ_L^{n+1} can be solved from summing up all equations (with suitable weights) in (5.20). Once ρ_L^{n+1} is available, $g_{L,v}^{n+1}$ for all discrete v can be obtained.

In this paper, we only consider boundary conditions that do not lead to either boundary layers due to anisotropic boundary data [23] or corner singularities due to the incompatibility of initial and boundary conditions [13]. These interesting and challenging problems are subject to our future investigation. Initially, with given ρ_h^0, g_h^0 and $f_L(v,0)$, ρ_L^0 and g_L^0 can be directly obtained from (5.20) with $n+1$ to be 0. In the following, we apply the proposed DG-IMEX schemes to several numerical examples. The time step is defined in the same way as in Section 4, except that we take $C_{hyper} = 1/3$ and $C_{diff} = 2/3$ for IMEX1 [16].

5.1 Smooth example with periodic boundary conditions

We consider the following initial conditions

$$\begin{cases} \rho(x,0) = 2 + \sin(x), \\ g(x,v,0) = -v\cos(x). \end{cases} \tag{5.21}$$

on the computational domain $[-\pi, \pi]$ with periodic boundary conditions. We take $\sigma_S = 1$ and $\sigma_A = G = 0$ uniformly. The initial conditions satisfy the limiting equilibrium equation, that is, we have $g = -v\rho_x$. The v direction is discretized with the standard 16-point Gaussian quadrature set on the whole set $[-1, 1]$ (see [24]). The simulation is run up to time $T = 0.1$ to test the orders of accuracy of the schemes. In Tables 5.15-5.17, we show the errors and orders of accuracy with $\varepsilon = 0.5, 10^{-2}, 10^{-6}$ for DG(k+1)-IMEX(k+1), k=0, 1, 2; the errors and orders are computed as specified in (4.5) and (4.6). For all three ε's, a uniform $(k+1)^{th}$ order of convergence is observed for DG(k+1)-IMEX(k+1). The results from DG(k+1)-IMEX(k+1) using central flux are presented in Tables 5.18-5.20. For all three ε's, a uniform $(k+1)^{th}$ order for even k and at least k^{th} order for odd k are observed. The observed convergence orders are similar to those for the telegraph equation.

5.2 Kinetic regime with isotropic boundary conditions [24].

In this example, we consider the computational domain $x \in [0, 1]$ with the initial condition $f(x, v, 0) = 0$ and the Dirichlet boundary conditions $f_L(v, t) = 0$, $f_R(v, t) = 1$. The parameters are specified as

$$\sigma_S = 1, \quad \sigma_A = 0, \quad G = 0, \quad \varepsilon = 1. \tag{5.22}$$

We discretize the velocity with 32-point Gaussian quadrature set for $[-1, 0]$ and for $[0, 1]$, separately. We plot the results in Figure 5.6 at times $t = 0.1, 0.4, 1.0, 1.6$, and 4. The symbols are with mesh size $\Delta x = 0.02$. The results are in good agreement with the reference solutions from DG1 with the explicit Euler forward time discretization by using $N = 1000$ points in the x direction and 64-point Gaussian quadrature set for $[-1, 0]$ and for $[0, 1]$. Higher order schemes are shown to have better resolution.

Table 5.15: L^1 errors and orders for ρ and $\langle vg \rangle$ for the one-group transport equation with initial conditions (5.21), $T = 0.1$, DG1-IMEX1 with alternating left-right flux.

	N	L^1 errors of ρ	order	L^1 error of $\langle vg \rangle$	order
$\varepsilon = 0.5$	10	9.31E-02	–	3.26E-02	–
	20	4.84E-02	0.94	1.64E-02	0.99
	40	2.42E-02	1.00	8.28E-03	0.98
	80	1.21E-02	1.00	4.15E-03	1.00
	160	6.04E-03	1.00	2.08E-03	1.00
$\varepsilon = 10^{-2}$	10	9.30E-02	–	3.46E-02	–
	20	4.85E-02	0.94	1.68E-02	1.04
	40	2.42E-02	1.00	8.25E-03	1.03
	80	1.21E-02	1.00	4.08E-03	1.01
	160	6.05E-03	1.00	2.03E-03	1.01
$\varepsilon = 10^{-6}$	10	9.30E-02	–	3.45E-02	–
	20	4.85E-02	0.94	1.68E-02	1.04
	40	2.42E-02	1.00	8.22E-03	1.03
	80	1.21E-02	1.00	4.07E-03	1.01
	160	6.05E-03	1.00	2.02E-03	1.01

Table 5.16: L^1 errors and orders for ρ and $\langle vg \rangle$ for the one-group transport equation with initial conditions (5.21), $T = 0.1$, DG2-IMEX2 with alternating left-right flux.

	N	L^1 errors of ρ	order	L^1 error of $\langle vg \rangle$	order
$\varepsilon = 0.5$	10	9.07E-03	–	4.28E-03	–
	20	2.83E-03	1.68	1.10E-03	1.96
	40	8.11E-04	1.81	2.47E-04	2.15
	80	1.93E-04	2.07	6.09E-05	2.02
	160	4.78E-05	2.01	1.51E-05	2.01
$\varepsilon = 10^{-2}$	10	1.12E-02	–	3.86E-03	–
	20	2.86E-03	1.97	9.54E-04	2.01
	40	7.08E-04	2.01	2.36E-04	2.01
	80	1.77E-04	2.00	5.89E-05	2.00
	160	4.41E-05	2.00	1.47E-05	2.00
$\varepsilon = 10^{-6}$	10	1.12E-02	–	3.85E-03	–
	20	2.85E-03	1.98	9.54E-04	2.01
	40	7.08E-04	2.01	2.36E-04	2.01
	80	1.77E-04	2.00	5.89E-05	2.00
	160	4.41E-05	2.00	1.47E-05	2.00

Table 5.17: L^1 errors and orders for ρ and $\langle vg \rangle$ for the one-group transport equation with initial conditions (5.21), $T = 0.1$, DG3-IMEX3 with alternating left-right flux.

	N	L^1 errors of ρ	order	L^1 error of $\langle vg \rangle$	order
$\varepsilon = 0.5$	10	5.02E-04	–	3.25E-04	–
	20	7.37E-05	2.77	3.10E-05	3.39
	40	1.02E-05	2.85	3.41E-06	3.19
	80	1.28E-06	2.99	4.11E-07	3.05
	160	1.62E-07	2.98	5.19E-08	2.99
$\varepsilon = 10^{-2}$	10	5.74E-04	–	2.20E-04	–
	20	7.65E-05	2.91	2.55E-05	3.11
	40	9.53E-06	3.00	3.18E-06	3.00
	80	1.19E-06	3.00	3.97E-07	3.00
	160	1.49E-07	3.00	4.96E-08	3.00
$\varepsilon = 10^{-6}$	10	5.75E-04	–	2.18E-04	–
	20	7.65E-05	2.91	2.55E-05	3.09
	40	9.53E-06	3.00	3.18E-06	3.00
	80	1.19E-06	3.00	3.97E-07	3.00
	160	1.49E-07	3.00	4.96E-08	3.00

Table 5.18: L^1 errors and orders for ρ and $\langle vg \rangle$ for the one-group transport equation with initial conditions (5.21), $T = 0.1$, DG1-IMEX1 with central flux.

	N	L^1 errors of ρ	order	L^1 error of $\langle vg \rangle$	order
$\varepsilon = 0.5$	10	9.31E-02	–	3.26E-02	–
	20	4.84E-02	0.94	1.64E-02	0.99
	40	2.42E-02	1.00	8.28E-03	0.98
	80	1.21E-02	1.00	4.15E-03	1.00
	160	6.04E-03	1.00	2.08E-03	1.00
$\varepsilon = 10^{-2}$	10	9.30E-02	–	3.20E-02	–
	20	4.85E-02	0.94	1.61E-02	0.99
	40	2.42E-02	1.00	8.06E-03	1.00
	80	1.21E-02	1.00	4.03E-03	1.00
	160	6.05E-03	1.00	2.02E-03	1.00
$\varepsilon = 10^{-6}$	10	9.30E-02	–	3.20E-02	–
	20	4.85E-02	0.94	1.61E-02	0.99
	40	2.42E-02	1.00	8.06E-03	1.00
	80	1.21E-02	1.00	4.03E-03	1.00
	160	6.05E-03	1.00	2.01E-03	1.00

Table 5.19: L^1 errors and orders for ρ and $\langle vg \rangle$ for the one-group transport equation with initial conditions (5.21), $T = 0.1$, DG2-IMEX2 with central flux.

	N	L^1 errors of ρ	order	L^1 error of $\langle vg \rangle$	order
$\varepsilon = 0.5$	10	7.92E-03	–	5.40E-03	–
	20	2.36E-03	1.75	1.97E-03	1.46
	40	8.70E-04	1.44	6.05E-04	1.70
	80	3.98E-04	1.13	1.67E-04	1.86
	160	1.99E-04	1.00	4.34E-05	1.94
	320	1.01E-04	0.98	1.10E-05	1.97
$\varepsilon = 10^{-2}$	10	9.15E-03	–	2.39E-02	–
	20	3.10E-03	1.56	1.19E-02	1.01
	40	1.11E-03	1.48	5.50E-03	1.11
	80	3.73E-04	1.58	2.36E-03	1.22
	160	9.36E-05	1.99	9.21E-04	1.36
	320	2.06E-05	2.19	3.21E-04	1.52
$\varepsilon = 10^{-6}$	10	9.32E-03	–	2.52E-02	–
	20	3.44E-03	1.44	1.31E-02	0.94
	40	1.50E-03	1.20	6.62E-03	0.99
	80	7.19E-04	1.06	3.32E-03	1.00
	160	3.55E-04	1.02	1.66E-03	1.00
	320	1.77E-04	1.00	8.30E-04	1.00

Table 5.20: L^1 errors and orders for ρ and $\langle vg \rangle$ for the one-group transport equation with initial conditions (5.21), $T = 0.1$, DG3-IMEX3 with central flux.

	N	L^1 errors of ρ	order	L^1 error of $\langle vg \rangle$	order
$\varepsilon = 0.5$	10	4.53E-04	–	2.00E-04	–
	20	5.94E-05	2.93	1.85E-05	3.44
	40	7.14E-06	3.06	2.07E-06	3.16
	80	8.74E-07	3.03	2.57E-07	3.01
	160	1.08E-07	3.02	3.21E-08	3.01
$\varepsilon = 10^{-2}$	10	4.41E-04	–	1.45E-04	–
	20	5.05E-05	3.13	1.68E-05	3.12
	40	6.12E-06	3.04	2.03E-06	3.04
	80	7.56E-07	3.02	2.51E-07	3.02
	160	9.41E-08	3.01	3.13E-08	3.01
$\varepsilon = 10^{-6}$	10	4.39E-04	–	1.45E-04	–
	20	5.03E-05	3.13	1.68E-05	3.12
	40	6.10E-06	3.04	2.03E-06	3.04
	80	7.54E-07	3.02	2.51E-07	3.02
	160	9.39E-08	3.01	3.13E-08	3.01

5.3 Two-material problem at stationary time [24, 22, 20]

We consider the computational domain with $x \in [0, 11]$. The initial and boundary conditions, as well as parameters, are specified as following,

$$\begin{aligned} f_L(v,t) = 5, \quad f_R(v,t) = 0, \quad \varepsilon = 1, \\ \sigma_S = 0, \quad \sigma_A = 1, \quad G = 0, \quad \text{for } x \in [0,1], \\ \sigma_S = 100, \quad \sigma_A = 0, \quad G = 0, \quad \text{for } x \in [1,11]. \end{aligned} \tag{5.23}$$

A diffusion regime is obtained after sufficiently long time when the scattering coefficient $\sigma_S = 100$ in the domain $[1, 11]$. An interface layer is produced between the absorbing region $[0, 1]$ and the scattering region $[1, 11]$. Under the DG framework, we use two different meshes sizes that are adaptive to the solution structure with $\Delta x = 0.025$ in $[0, 1]$ and $\Delta x = 0.5$ in $[1, 11]$. The v discretization is the same as Example 5.2. The reference solution is obtained with the DG1 with the explicit Euler forward time discretization using $N = 2000$ points. We run the simulation to a steady state with the final time $t = 20000$. The results are plotted in Figure 5.7. We can see the results all match well the reference solution, and high order results are better than the first order one.

5.4 Spatially varying σ_S at stationary time [12]

Finally, we consider an example from [12] with $f_L(v,t) = 3$ and $f_R(v,t) = 0$ on the spatial domain $[0, 1]$. The initial condition is $f(x, v, 0) = 3x^2$. We take $\sigma_S = 2$ for $x < 0.45$, $\sigma_S = 100$ for $x > 0.55$, and a linear interpolation of 2 and 100 for $0.45 \le x \le 0.55$. For this problem, the region $[0, 0.45]$ is in the kinetic regime and $[0.55, 1]$ is in the diffusive regime. Here $\sigma_A = G = 0$. We show in Figure 5.8 the numerical solutions at the steady state with the final time $t = 1000$. The results with $N = 25$ match very well the reference solution with $N = 1000$ and the results in [12]. Here the v discretization is also the same as Example 5.2.

6 Conclusion

This paper is an initial effort in developing high order asymptotic preserving schemes for kinetic equations in different scalings. For some discrete-velocity kinetic models in a diffusive scaling, we propose to employ arbitrarily high order DG spatial discretizations coupled with high order globally stiffly accurate IMEX scheme for an equivalent micro-macro decomposition of the kinetic equations. The proposed schemes are asymptotic preserving in the sense of [18]. Moreover, they are of high order in both space and time when ε is of order 1 and in the limit of $\varepsilon \to 0$. The methods also naturally extend to the continuous-velocity one-group transport equation in slab geometry. Some uniform stability analysis and error estimates for the proposed schemes are rigorously established in a separate paper [16]. Extensions to more general kinetic equations with different asymptotic limits will be explored in the future.

Acknowledgement. This project was initiated during the authors' participation at the ICERM Semester Program on "Kinetic Theory and Computation" in the fall of 2011. The authors want to thank for the generous support from the Institute. Part of the work was done at MFO in Oberwolfach during a Research in Pairs program. The first three authors appreciate the support and hospitality of the Institute.

References

[1] U. Ascher, S. Ruuth, and R. Spiteri, *Implicit-explicit Runge-Kutta methods for time-dependent partial differential equations*, Applied Numerical Mathematics, 25 (1997), pp. 151–167.

[2] C. Bardos, F. Golse, and D. Levermore, *Fluid dynamic limits of kinetic equations. i. formal derivations*, Journal of statistical physics, 63 (1991), pp. 323–344.

[3] S. Boscarino, *Error analysis of IMEX Runge-Kutta methods derived from differential-algebraic systems*, SIAM Journal on Numerical Analysis, 45 (2008), pp. 1600–1621.

[4] S. Boscarino, L. Pareschi, and G. Russo, *Implicit-explicit Runge–Kutta schemes for hyperbolic systems and kinetic equations in the diffusion limit*, SIAM Journal on Scientific Computing, 35 (2013), pp. A22–A51.

[5] S. Boscarino and G. Russo, *On a class of uniformly accurate IMEX Runge-Kutta schemes and applications to hyperbolic systems with relaxation*, SIAM Journal on Scientific Computing, 31 (2009), pp. 1926–1945.

[6] S. Boscarino and G. Russo, *Flux-explicit IMEX Runge–Kutta schemes for hyperbolic to parabolic relaxation problems*, SIAM Journal on Numerical Analysis, 51 (2013), pp. 163–190.

[7] J. Bourgat, P. Le Tallec, B. Perthame, and Y. Qiu, *Coupling Boltzmann and Euler equations without overlapping*, Contemporary Mathematics, 157 (1994), pp. 377–377.

[8] J. A. Carrillo, T. Goudon, P. Lafitte, and F. Vecil, *Numerical schemes of diffusion asymptotics and moment closures for kinetic equations*, Journal of Scientific Computing, 36 (2008), pp. 113–149.

[9] B. Cockburn and C.-W. Shu, *The local discontinuous Galerkin method for time-dependent convection-diffusion systems*, SIAM Journal on Numerical Analysis, 35 (1998), pp. 2440–2463.

[10] ——, *Runge–Kutta discontinuous Galerkin methods for convection-dominated problems*, Journal of Scientific Computing, 16 (2001), pp. 173–261.

[11] J.-F. Coulombel, F. Golse, and T. Goudon, *Diffusion approximation and entropy-based moment closure for kinetic equations*, Asymptotic Analysis, 45 (2005), pp. 1–39.

[12] P. Degond and S. Jin, *A smooth transition model between kinetic and diffusion equations*, SIAM journal on numerical analysis, 42 (2005), pp. 2671–2687.

[13] N. Flyer and B. Fornberg, *Accurate numerical resolution of transients in initial-boundary value problems for the heat equation*, Journal of Computational Physics, 184 (2003), pp. 526–539.

[14] J.-L. Guermond and G. Kanschat, *Asymptotic analysis of upwind discontinuous Galerkin approximation of the radiative transport equation in the diffusive limit*, SIAM Journal on Numerical Analysis, 48 (2010), pp. 53–78.

[15] J. S. Hesthaven and T. Warburton, *Nodal discontinuous Galerkin methods: algorithms, analysis, and applications*, vol. 54, Springerverlag New York, 2008.

[16] J. Jang, F. Li, J.-M. Qiu, and T. Xiong, *Analysis of asymptotic preserving DG-IMEX schemes for linear kinetic transport equations in a diffusive scaling*, SIAM Journal on Numerical Analysis, 52 (2014), pp. 1497–2206.

[17] G.-S. Jiang, , and C.-W. Shu, *On a cell entropy inequality for discontinuous Galerkin methods*, Mathematics of Computation, 62 (1994), pp. 531–538.

[18] S. Jin, *Asymptotic preserving (AP) schemes for multiscale kinetic and hyperbolic equations: a review*, Lecture Notes for Summer School on Methods and Models of Kinetic Theory M&MKT), Porto Ercole (Grosseto, Italy), (2010).

[19] S. Jin and C. Levermore, *Numerical schemes for hyperbolic conservation laws with stiff relaxation terms*, Journal of computational physics, 126 (1996), pp. 449–467.

[20] S. Jin, L. Pareschi, and G. Toscani, *Diffusive relaxation schemes for multiscale discrete-velocity kinetic equations*, SIAM Journal on Numerical Analysis, 35 (1998), pp. 2405–2439.

[21] ——, *Uniformly accurate diffusive relaxation schemes for multiscale transport equations*, SIAM Journal on Numerical Analysis, 38 (2000), pp. 913–936.

[22] A. Klar, *An asymptotic-induced scheme for nonstationary transport equations in the diffusive limit*, SIAM journal on numerical analysis, 35 (1998), pp. 1073–1094.

[23] M. Lemou and F. Méhats, *Micro-macro schemes for kinetic equations including boundary layers*, SIAM Journal on Scientific Computing, 34 (2012), pp. B734–B760.

[24] M. Lemou and L. Mieussens, *A new asymptotic preserving scheme based on micro-macro formulation for linear kinetic equations in the diffusion limit*, SIAM Journal on Scientific Computing, 31 (2008), pp. 334–368.

[25] C. D. Levermore, *Moment closure hierarchies for kinetic theories*, Journal of Statistical Physics, 83 (1996), pp. 1021–1065.

[26] J. Liu and L. Mieussens, *Analysis of an Asymptotic Preserving Scheme for Linear Kinetic Equations in the Diffusion Limit*, SIAM Journal on Numerical Analysis, 48 (2010), pp. 1474–1491.

[27] T.-P. Liu and S.-H. Yu, *Boltzmann equation: micro-macro decompositions and positivity of shock profiles*, Communications in mathematical physics, 246 (2004), pp. 133–179.

[28] G. Naldi and L. Pareschi, *Numerical schemes for kinetic equations in diffusive regimes*, Applied mathematics letters, 11 (1998), pp. 29–35.

[29] L. Pareschi and G. Russo, *Implicit–explicit Runge–Kutta schemes and applications to hyperbolic systems with relaxation*, Journal of Scientific computing, 25 (2005), pp. 129–155.

[30] ——, *Efficient asymptotic preserving deterministic methods for the Boltzmann equation in Models and Computational Methods for Rarefied Flows*, Lecture Series held at the von Karman Institute,Rhode St. Gense, Belgium, AVT-194 RTO AVT/VKI, (2011).

[31] B. Rivière, *Discontinuous Galerkin methods for solving elliptic and parabolic equations: theory and implementation*, SIAM, Philadelphia, 2008.

[32] T. Ruijgrok and T. Wu, *A completely solvable model of the nonlinear Boltzmann equation*, Physica A: Statistical Mechanics and its Applications, 113 (1982), pp. 401–416.

[33] L. Saint-Raymond, *Hydrodynamic limits of the Boltzmann equation*, Springer-Verlag, Berlin, 2009.

[34] Y. Xu and C.-W. Shu, *Local discontinuous Galerkin methods for high-order time-dependent partial differential equations*, Communications in Computational Physics, 7 (2010), pp. 1–46.

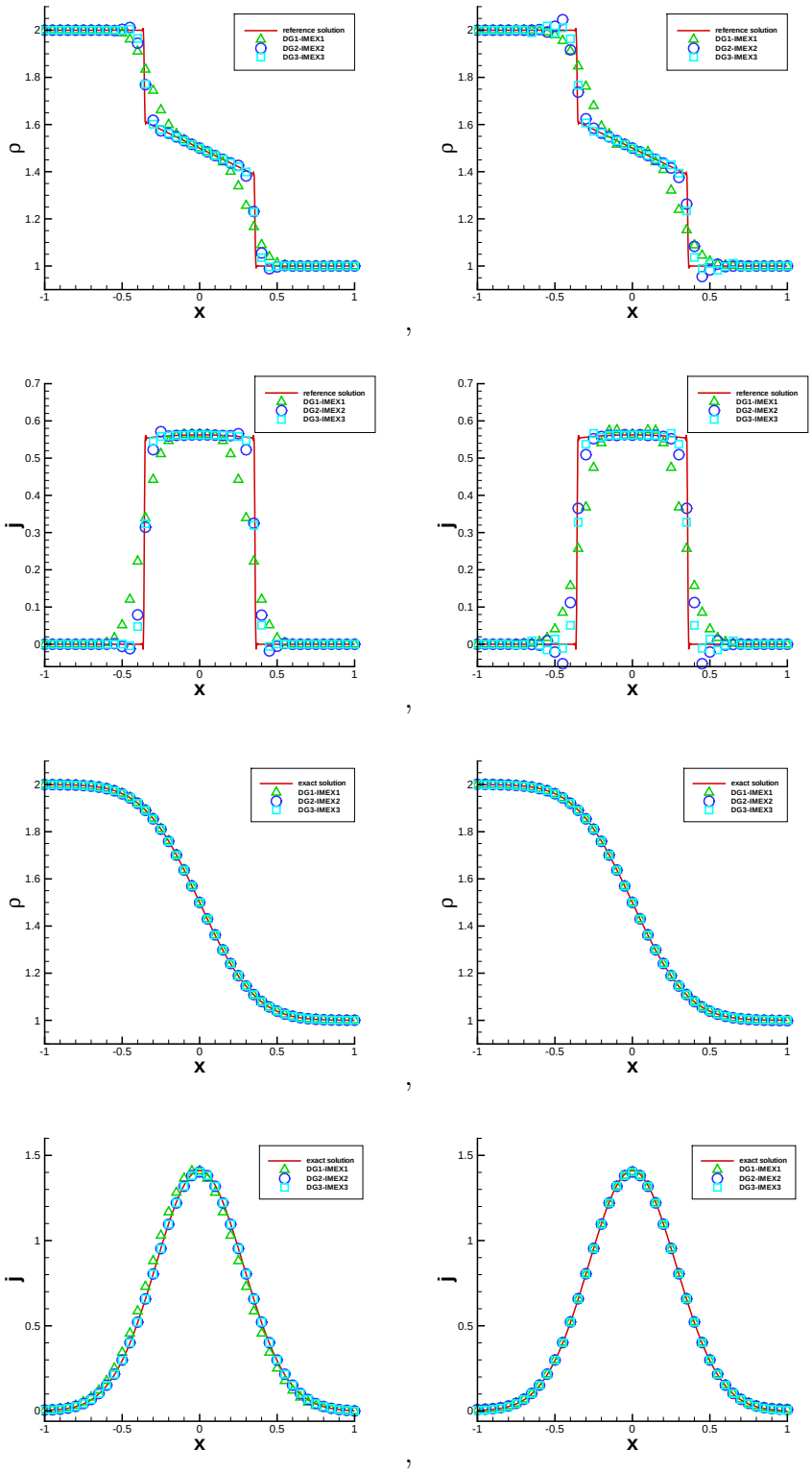

Figure 4.1: Numerical solutions of the telegraph equation with initial conditions (4.2) by DG(k+1)-IMEX(k+1), $k = 0, 1, 2$ in the rarefied regime $\varepsilon = 0.7$ at $T = 0.25$ (top two rows) and in the parabolic regime $\varepsilon = 10^{-6}$ at $T = 0.04$ (bottom two rows). $\Delta x = 0.05$. Left: left-right flux; Right: central flux. The reference solutions are obtained by DG3-IMEX3 with $\Delta x = 0.004$, with the left-right flux for the left column, and the central flux for the right column.

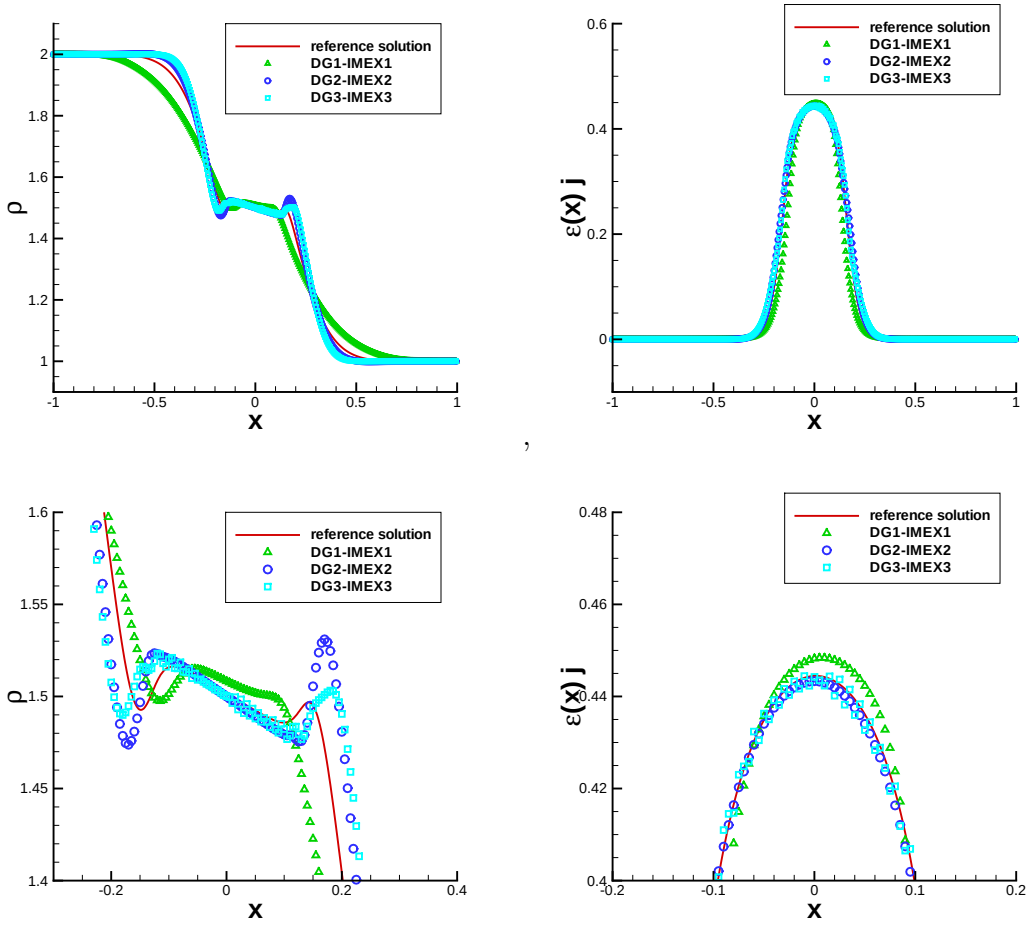

Figure 4.2: Numerical solutions of the telegraph equation with initial conditions (4.2) by DG(k+1)-IMEX(k+1), $k = 0, 1, 2$ at $T = 0.06$. $\Delta x = 0.005$. The reference solutions are obtained by DG1 with Euler forward time discretization on the mesh size $\Delta x = 5 \times 10^{-5}$. Alternating left-right flux is used. Bottom are zoom-in figures of the top ones.

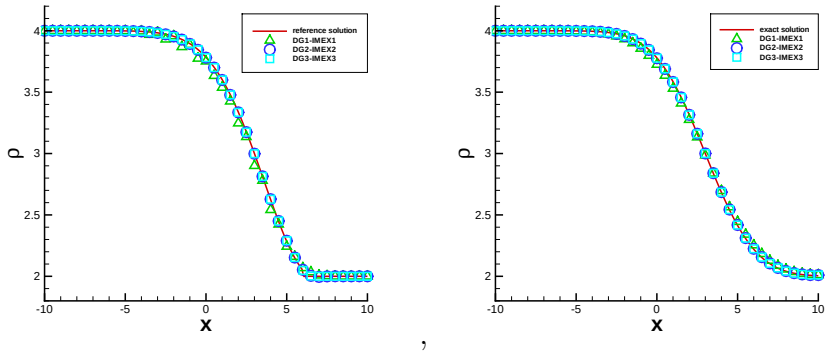

Figure 4.3: Numerical solutions of the advection-diffusion equation with initial conditions (4.9) by DG(k+1)-IMEX(k+1), $k = 0, 1, 2$ at $T = 3.0$. Left-right flux and $\Delta x = 0.5$. Left: the rarefied regime $\varepsilon = 0.5$; Right: the parabolic regime $\varepsilon = 10^{-6}$.

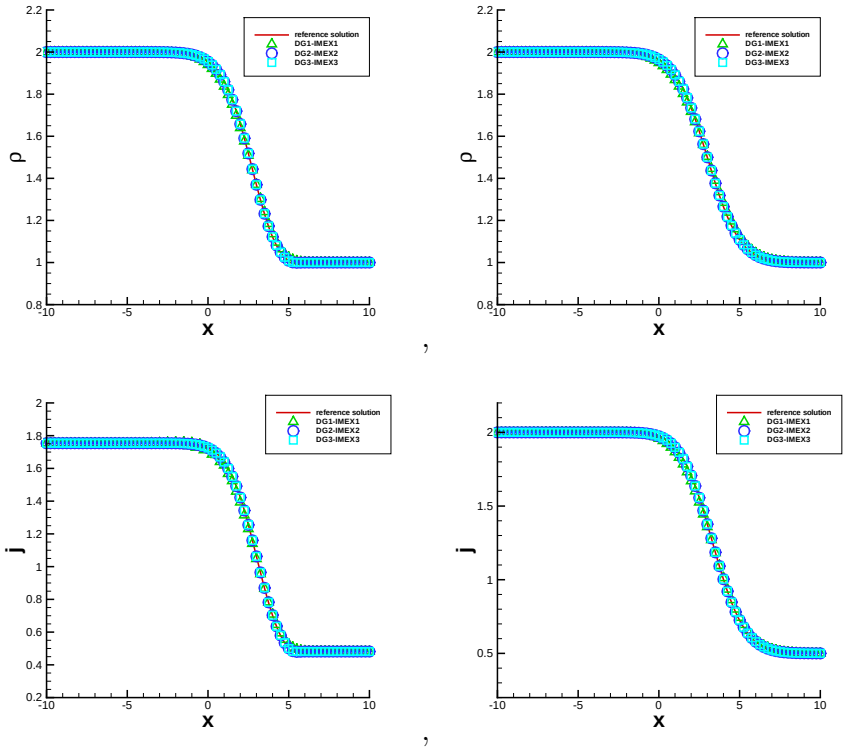

Figure 4.4: Numerical solutions of the viscous Burgers' equation with initial conditions (4.11) by DG(k+1)-IMEX(k+1), $k = 0, 1, 2$ at $T = 2.0$. Left-right flux and $\Delta x = 0.25$. Left: the rarefied regime $\varepsilon = 0.4$; Right: the parabolic regime $\varepsilon = 10^{-6}$. Symbol: numerical solution; Solid line: reference solution.

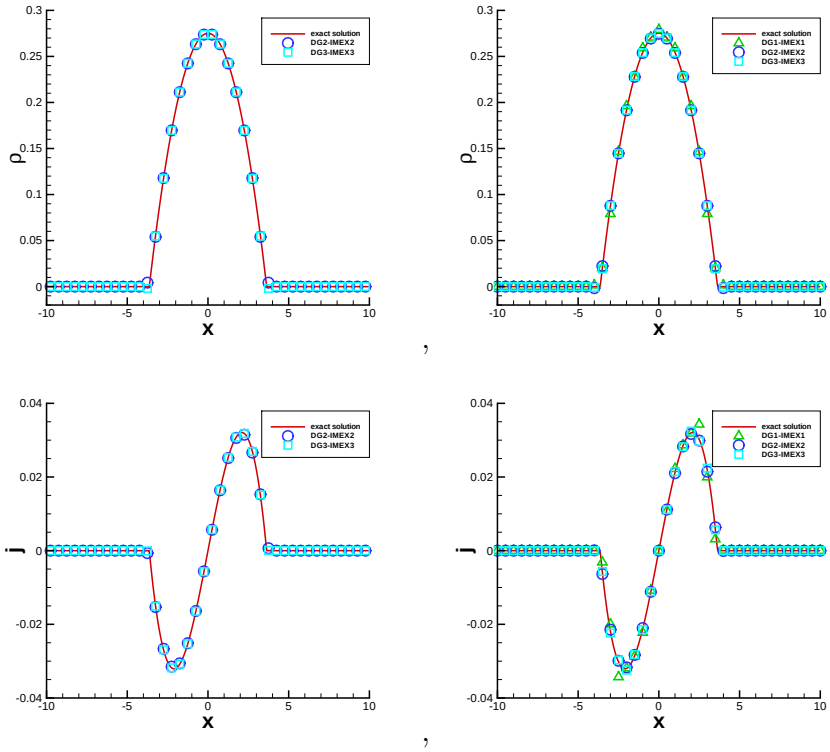

Figure 4.5: Numerical solutions of the porous media equation compared with the limiting Barenblatt solution (4.15). The parabolic regime $\varepsilon = 10^{-6}$ at $T = 3.0$ with $\Delta x = 0.5$. Left: alternating flux; Right: central flux.

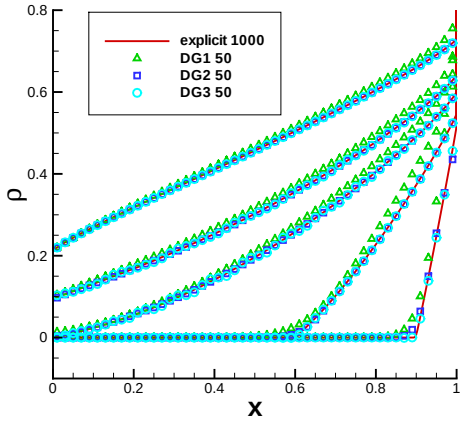

Figure 5.6: Numerical solutions of the one-group transport equation for Example 5.2 with parameters (5.22) by DG(k+1)-IMEX(k+1), $k = 0, 1, 2$ at $T = 0.1, 0.4, 1.0, 1.6, 4$. $\Delta x = 0.02$. The reference solutions are obtained by DG1 with explicit Euler forward time discretization on the mesh size $\Delta x = 0.001$ ($N = 1000$). Alternating left-right flux is used.

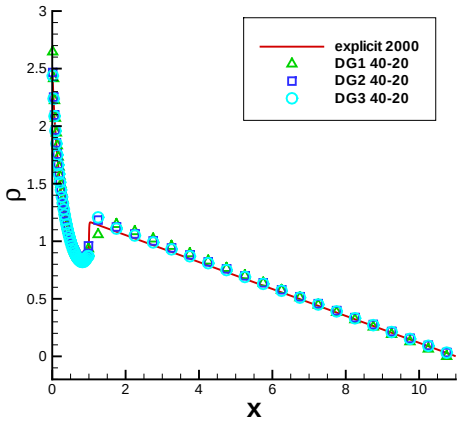

Figure 5.7: Numerical solutions of the one-group transport equation for Example 5.3 with parameters (5.23) by DG(k+1)-IMEX(k+1), $k = 0, 1, 2$ at $T = 20000$. The symbols are numerical solutions with $\Delta x = 0.025$ in $[0, 1]$ and $\Delta x = 0.5$ in $[1, 11]$. The reference solutions are obtained by DG1 with Euler forward time discretization on the mesh size $\Delta x = 0.0055$ ($N = 2000$). Alternating left-right flux is used.

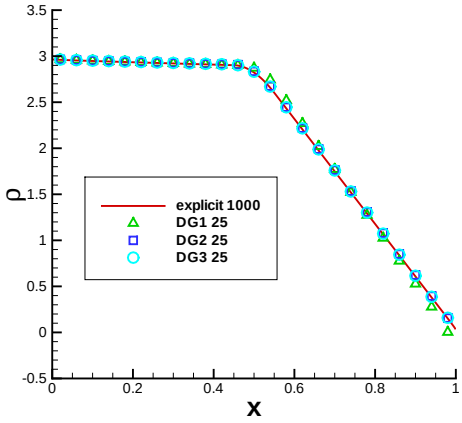

Figure 5.8: Numerical solutions of the one-group transport equation for Example 5.4 by DG(k+1)-IMEX(k+1), $k = 0, 1, 2$ at $T = 1000$. The symbols are numerical solutions with $\Delta x = 0.04$ ($N = 25$). The reference solutions are obtained by DG1 with Euler forward time discretization on the mesh size $\Delta x = 0.001$ ($N = 1000$). Alternating left-right flux is used.